

We are IntechOpen, the world's leading publisher of Open Access books Built by scientists, for scientists

6,900

Open access books available

186,000

International authors and editors

200M

Downloads

Our authors are among the

154

Countries delivered to

TOP 1%

most cited scientists

12.2%

Contributors from top 500 universities



WEB OF SCIENCE™

Selection of our books indexed in the Book Citation Index
in Web of Science™ Core Collection (BKCI)

Interested in publishing with us?
Contact book.department@intechopen.com

Numbers displayed above are based on latest data collected.
For more information visit www.intechopen.com



Photocatalytic Removal of Organics over BiVO₄-Based Photocatalysts

Kunfeng Zhang, Jiguang Deng, Yuxi Liu,
Shaohua Xie and Hongxing Dai

Additional information is available at the end of the chapter

<http://dx.doi.org/10.5772/62745>

Abstract

Organic compounds, such as organic dyes and phenols, are the main pollutants in wastewater. In the past years, a large number of studies on the fabrication and photocatalytic organics degradation of BiVO₄ and its related materials have been reported in the literature. In this chapter, we shall focus on the advancements in the synthesis and photocatalytic applications of several kinds of BiVO₄-based photocatalysts: (i) well-defined morphological BiVO₄ photocatalysts, (ii) porous BiVO₄ photocatalysts, (iii) heteroatom-doped BiVO₄ photocatalysts, (iv) BiVO₄-based heterojunction photocatalysts, and (v) supported BiVO₄ photocatalysts. We shall discuss the structure–photocatalytic performance relationship of the materials and the involved photocatalytic degradation mechanisms. In addition, we also propose the research trends and technologies for practical applications of the BiVO₄-based photocatalytic materials.

Keywords: well-defined morphology, porous BiVO₄ photocatalyst, heteroatom-doped BiVO₄, BiVO₄-based heterojunction, supported BiVO₄

1. Introduction

With the unceasingly expanding industrial development, environmental pollution caused by industrial effluents has nowadays become the most urgent issue to be solved [1]. In particular, various industrial processes and human activities contaminate the global water supply, which is a serious problem for living beings. During the past decades, great efforts have been made on the degradation of organic wastewater pollutants. The visible-light-driven photoca-

talysis attracts much attention, since such a photocatalytic process can directly convert organic pollutants (e.g., methylene blue (MB), methyl orange (MO), rhodamine B (RhB), phenol, and etc.) to harmless products (CO_2 and H_2O) under sunlight irradiation.

The organic dye models (MB, MO, and RhB) in textile and other industrial effluents have become one series of the major environmental contaminants, which have serious implications on the environment and human health [2]. Meanwhile, phenol is a widely used chemical and present in a great variety of emitted waste effluents. Organic dyes and phenol degrade slowly in the environment and are extremely toxic, carcinogenic, teratogenic, and refractory in nature [3]. Therefore, tremendous efforts have been made to fabricate high-efficiency photocatalysts for the control of wastewater pollution.

As one of the earliest studied *n*-type semiconductor photocatalysts, TiO_2 has been widely used in environmental purification owing to its appropriate band position, high chemical stability, low cost, and nontoxicity [4]. However, TiO_2 is only responsive to ultraviolet (UV) light owing to its wide bandgap energy (3.2 eV), which occupies no more than 4% of the solar spectrum, hence greatly restricting its practical applications [5]. Among the developed catalysts, BiVO_4 is one of the most attractive photocatalysts due to its unique properties, such as ferroelasticity, photochromic effect, ionic conductivity, and visible-light responsibility [6]. It is nontoxic and has a relatively narrow bandgap energy (2.4 eV) when it is monoclinic in crystal structure. Many publications on BiVO_4 describing phase structures, synthesis methods, physicochemical properties, applications, and so on have emerged since its inaugural work by Kudo et al. as a photocatalyst for O_2 evolution in 1999 [7]. As a promising material, BiVO_4 is extensively applied in various fields, such as gas sensors, batteries, electrolytes, water splitting, and other applications [8].

Semiconductor is a kind of materials with electrical conductivity between conductor (such as metals) and insulator (such as ceramics). The unique electronic property of a semiconductor is characterized by its valence band (VB) and conduction band (CB). The VB of a semiconductor is formed by the interaction of the highest occupied molecular orbital (HOMO), while the CB is formed by the interaction of the lowest unoccupied molecular orbital (LUMO). There is no electron state between the top of the VB and the bottom of CB. The energy range between CB and VB is called forbidden bandgap (also called bandgap energy), which is usually denoted as E_g . The band structure, including the bandgap and the positions of VB and CB, is one of the important properties for a semiconductor photocatalyst, because it determines the light absorption property as well as the redox capability of a semiconductor [9].

As shown in reaction 1, the photocatalytic reaction initiates from the generation of electron–hole pairs upon light irradiation. When a semiconductor photocatalyst absorbs photons with energy equal to or greater than its E_g , the electrons in the VB will be excited to the CB, leaving the holes in the VB. The electron-hole pairs generation process in BiVO_4 can be expressed as follows:



These photogenerated electron–hole pairs may further be involved in the following three possible processes [9]: (i) successfully migrating to the surface of semiconductor, (ii) being captured by the defect sites in bulk and/or on the surface region of semiconductor, and (iii) recombining and releasing the energy in the form of heat or photon. The last two processes are generally viewed as deactivation processes because the photogenerated electrons and holes do not contribute to the photocatalytic reactions. Only the photogenerated charges that reach to the surface of semiconductor can be available for photocatalytic reactions. The defect sites in the bulk and on the surface of semiconductor may serve as the recombination centers for the photogenerated electrons and holes, which would decrease the efficiency of the photocatalytic reaction.

It is well known that the photocatalytic activity of a semiconductor depends strongly upon three factors: adsorption behavior, photoresponsive region, and separation efficiency of electron–hole pairs [10]. The adsorption behavior can usually be enhanced by improving the surface areas of catalysts. In this aspect, how to extend the photoresponsive region and improve the separation efficiency of electron–hole pairs are important factors on the photocatalytic performance of a semiconductor [11]. The way to extend the photoresponsive region of a semiconductor photocatalyst is mainly the doping of nonmetals or transition metals, which can also improve the separation efficiency of electron–hole pairs and increase the oxidation power of photogenerated carriers [12, 13]. In general, noble metals (e.g., Ag, Pt, Au, and Pd) have been used as electron acceptors to separate the photoinduced hole–electron pairs and promote the interfacial charge transfer processes [14].

Generally speaking, physicochemical properties of a material may be quite different depending on its crystal phase structure. The phase structure of BiVO₄ is one of the important factors determining its photocatalytic performance [15]. BiVO₄ has mainly three polymorphs in nature, including zircon–tetragonal, scheelite–tetragonal, and scheelite–monoclinic. The zircon–tetragonal phase can be formed via a low-temperature (100°C) synthesis route, whereas the scheelite–monoclinic phase can be generated using a high-temperature (400–600°C) synthesis method [16]. Moreover, the phase transformation between the scheelite monoclinic and the scheelite tetragonal can occur reversibly at 255°C [17]. It has been confirmed that the scheelite monoclinic structure of BiVO₄ is the most photocatalytically active under visible-light irradiation. The greater reactivity can be associated with the energy band structure since monoclinic and tetragonal BiVO₄ have bandgap energies of 2.4 and 2.9 eV, respectively. [8, 18, 19] Though BiVO₄ has better photocatalytic performance, various strategies have been proposed to further improve its activity. In addition to the crystal structure, the photocatalytic property also strongly depends upon the morphology of BiVO₄ [20]. Different morphological semiconductor photocatalysts have been prepared by many researchers. Efficient charge separation is the most important factor that determines the photocatalytic performance [9]. Furthermore, creation of heterjunction [21] and porous structure [22] as well as doping of element(s) [23] and using of support [24] are also effective strategies for improving charge separation efficiency.

2. Well-defined morphological BiVO₄ photocatalysts

As one of new photocatalysts, monoclinic BiVO₄ (*m*-BiVO₄) with a bandgap energy of 2.4 eV has drawn great attention for its excellent performance under visible-light illumination [7, 25]. Therefore, many strategies, such as solid-state reaction, hydrothermal or solvothermal, chemical bath deposition, and solution combustion methods, are employed for the synthesis of monoclinic BiVO₄. The morphology of a crystal plays a crucial role in determining its physicochemical property [26]. In recent years, scientists have been devoted to developing various synthetic routes to realize the tailored fabrication of *m*-BiVO₄ with different morphologies that show distinct photocatalytic properties [27]. For example, the hydrothermal method is widely used to prepare *m*-BiVO₄ with different morphologies because the morphology of the final product obtained via such a process can be easily controlled by changing the reaction conditions, such as reaction temperature, reaction time, solution pH, and concentration [6]. Recently, different morphologies (such as nanospheres, nanorods, nanoflowers, nanosheets, nanotubes, hyperbranched) of monoclinically structured BiVO₄ crystallites have been synthesized by the hydrothermal method with the assistance of surfactants and pH-controlling additives [28]. **Table 1** summarizes the physical properties and photocatalytic activities of the typical BiVO₄ reported in the literature.

Photocatalyst	Crystal structure	Surface area (m ² /g)	E _g (eV)	Reaction condition	Degradation efficiency and light illumination time	References
Sphere-like BiVO ₄	Monoclinic	1.75	–	Visible light, 80 mL RhB (0.01 mmol/L), 0.1 g sample	100% and 20 min	[2]
	Monoclinic	–	–	UV light, RhB	84.1% and 2.5 h	[6]
	Monoclinic	8.4	2.45	Visible light, 200 mL MO (0.01 mmol/L), 0.1 g sample	84% and 2 h	[22]
	Monoclinic	10	2.37	Sunlight, 50 mL phenol (25 mg/L), 0.3 mL H ₂ O ₂ , 0.1 g sample	100% and 1.5 h	[29]
	Monoclinic	2.62	2.48	Visible light, 100 mL RhB (0.01 mmol/L), 0.08 g sample	97.7% and 6 h	[30]
	Monoclinic	–	2.5	Visible light, 100 mL RhB, 0.01 g sample	80% and 50 min	[31]
	Tetragonal	–	2.81	Sunlight, 100 mL MB (5 mg/L), 0.1 g sample	90% and 5 h	[32]
	Monoclinic	24.4	2.50	Blue light, 50 mL MB (0.01 mmol/L), 0.005 g sample	100% and 5 h	[33]
	Monoclinic	85.4	2.38	Visible light, 20 mL MB (20 mg/L), 0.02 g sample	63% and 2 h	[34]

Photocatalyst	Crystal structure	Surface area (m ² /g)	E _g (eV)	Reaction condition	Degradation efficiency and light illumination time	References
	Monoclinic	0.7	2.42	Visible light, 100 mL MB (0.01 mmol/L), 0.01 g sample	90% and 3 h	[35]
Flower-like BiVO ₄	Monoclinic	0.9	2.3	Visible light, MB (10 mg/L), 1 g/L sample	60% and 2 h	[28]
	Monoclinic	61.6	2.14	Visible light, 20 mL MB (20 mg/L), 0.02 g sample	75% and 2 h	[34]
	Monoclinic	–	2.46	Sunlight, 100 mL MO (10 mg/L), 0.5 g sample	58% and 4 h	[36]
	Monoclinic	1.6	2.45	Sunlight, 200 mL RhB (5 mg/L), 0.1 g sample	62% and 10 h	[37]
	Monoclinic	2.1	2.52	Visible light, 100 mL MO (0.01 mmol/L), 0.1 g sample	60% and 4 h	[38]
Rod-like BiVO ₄	Monoclinic	3.5	2.46	Sunlight, 200 mL RhB (10 mg/L), 0.2 g sample	98.3% and 8 h	[27]
	Monoclinic	4.3	2.26	Visible light, 100 mL MB (0.01 mmol/L), 0.01 g sample	90% and 2 h	[35]
	Monoclinic	3.8	2.47	Visible light, 100 mL MO (0.01 mmol/L), 0.1 g sample	87% and 4 h	[38]
	Monoclinic/ tetragonal	–	2.46	Visible light, 100 mL RhB (10 mg/L), 0.04 g sample	39.5% and 2.5 h	[39]
	Monoclinic	–	2.45	Visible light, 100 mL RhB (0.01 mmol/L), 0.2 g sample	96% and 50 min	[40]
		Monoclinic	10.3	2.4	Sunlight, 200 mL RhB (5 mg/L), 0.1 g sample	61% and 10 h
Peanut-like BiVO ₄	Monoclinic	0.54	2.4	Solar light, 100 mL crystalviolet (0.02 mmol/L), 0.05 g sample	98% and 1 h	[41]
	Monoclinic	33.9	2.44	Visible light, 100 mL MB (10 mg/L), 0.1 g sample	95% and 225 min	[42]
	Monoclinic	5.4	2.35	UV-Vis light, 100 mL MB (10 ppm), 1 g/L sample	40% and 2 h	[43]
Polyhedron-like BiVO ₄	Monoclinic	0.9	2.34	Visible light, 100 mL MB (0.01 mmol/L), 0.01 g sample	90% and 2 h	[35]
	Monoclinic	3.97	2.25	Visible light, 50 mL RhB (0.015 mmol/L), 0.1 g sample	60% and 10 h	[44]
	Monoclinic	–	2.35	Visible light, 30 mL MB (5 mg/L), 0.1 g sample	81.6% and 160 min	[45]

Photocatalyst	Crystal structure	Surface area (m ² /g)	E _g (eV)	Reaction condition	Degradation efficiency and light illumination time	References
	Monoclinic	0.4	2.35	Visible light,alachlor (50 mg/L), 1 g/L sample	97% and 6 h	[46]
Olive-like BiVO ₄	Monoclinic	0.91	2.40	Sunlight, 50 mL MB (10 mg/L), 0.1 g sample	18% and 3.5 h	[26]
	Monoclinic	4.6	2.40	Sunlight, 200 mL RhB (5 mg/L), 0.1 g sample	97% and 10 h	[37]
	Monoclinic	–	2.50	Visible light, 100 mL RhB (10 mg/L), 0.04 g sample	50.5% and 2.5 h	[39]
	Monoclinic	–	2.45	Visible light, 100 mL MB (10 mg/L), 0.1 g sample	67% and 225 min	[42]
Microtube-like BiVO ₄	Monoclinic	6.6	2.33	Visible light, 100 mL MB (0.01 mmol/L), 0.01 g sample	90% and 3 h	[35]
	Monoclinic	–	2.36	Visible light, 100 mL RhB (0.01 mmol/L), 0.5 mmol sample	96% and 3 h	[47]
	Monoclinic	0.3	2.36	Visible light, MO (20 mg/L), 0.01 g sample	95% and 3 h	[48]
	Monoclinic	3.46	2.48	Visible light, 100 mL RhB (0.01 mmol/L), 0.2 g sample	100% and 5 h	[49]
Dumbbell-like BiVO ₄	Monoclinic	4.6	2.43	Visible light, 200 mL RhB (5 mg/L), 0.1 g sample	89% and 10 h	[37]
	Monoclinic	–	2.51	Visible light, 600 mL RhB (0.01 mmol/L), 0.3 g sample	90% and 4.5 h	[50]
	Monoclinic	9.87	2.25	Sunlight, 100 mL ofloxacin (20 mg/L), 0.1 g sample	80.8% and 1 h	[51]
	Monoclinic	53.6	2.42	Visible light, 100 mL RhB (0.01 mmol/L), 0.1 g sample	100% and 1 h	[52]
Needle-like BiVO ₄	Monoclinic	–	–	Sunlight, 200 mL RhB (5 mg/L), 0.1 g sample	40% and 10 h	[37]
	Monoclinic	2.0	2.41	UV-Vis light, MB (10 ppm), 1 g/L sample	60% and 2 h	[43]
	Monoclinic	17.63	2.42	Visible light, 100 mL MB (10 mg/L), 0.005 g sample	81% and 200 min	[53]
	Monoclinic	1.6	2.38	UV-Vis light, MB (10 ppm), 1 g/L sample	66% and 3 h	[54]
Dendrite-like BiVO ₄	Monoclinic/ tetragonal	1.88	2.52	Visible light, 100 mL MB (20 mg/L), 0.1 g sample	95% and 3 h	[16]

Photocatalyst	Crystal structure	Surface area (m ² /g)	E _g (eV)	Reaction condition	Degradation efficiency and light illumination time	References
Butterfly-like BiVO ₄	Monoclinic	1.22	2.34	Sunlight, 50 mL MB (10 mg/L), 0.1 g sample	74.8% and 3.5 h	[26]
Nanosheet-like BiVO ₄	Monoclinic	–	3.3	Visible light, 100 mL RhB, 0.01 g sample	50% and 50 min	[31]
Leaf-like BiVO ₄	Monoclinic	3.0	2.34	Visible light, 100 mL MB (0.01 mmol/L), 0.01 g sample	100% and 3 h	[35]
Cuboid-like BiVO ₄	Monoclinic	–	2.39	Sunlight, 100 mL MO (10 mg/L), 0.5 g sample	36% and 4 h	[36]
Star-like BiVO ₄	Monoclinic	–	2.44	Visible light, 100 mL MB (10 mg/L), 0.1 g sample	76% and 225 min	[42]
Bone-like BiVO ₄	Monoclinic	10.32	2.36	Visible light, 100 mL MB (0.01 mmol/L), 0.005 g sample	61% and 200 min	[53]

Table 1. Physical properties and photocatalytic activities of the well-defined morphological BiVO₄ photocatalysts.

2.1. Sphere-like BiVO₄

Among different morphologies of BiVO₄, microspherical or nanospherical BiVO₄ particles are mostly reported. For example, Kunduz et al. [29] reported the preparation of monoclinic bismuth vanadate catalysts by hydrothermal method at different pH values and the removal of phenol from wastewater under natural sunlight illumination. Homogenous and spherical BiVO₄ (particle size = 40–90 nm) was formed at pH = 2 (**Figure 1d**), the bandgap energy of the BiVO₄ sample calculated from the absorption edge was 2.37 eV. This BiVO₄ sample showed a high phenol conversion (100%) within 90 min of natural sunlight illumination, which was related to the morphology of BiVO₄ (surface area = 10 m²/g).

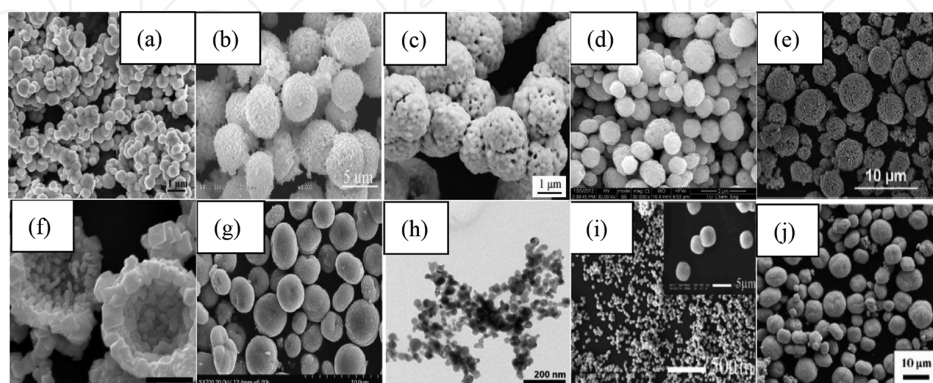


Figure 1. (a–g, i, j) SEM and (h) TEM images of sphere-like BiVO₄: (a) [2], (b) [6], (c) [22], (d) [29], (e) [30], (f) [31], (g) [32], (h) [33], (i) [34], and (j) [35].

An one-pot template-free hydrothermal method was developed for the fabrication of BiVO_4 microspheres with a tetragonal–monoclinic heterophasic structure [30]. The average diameter, bandgap energy, and BET surface area of the as-prepared BiVO_4 microspheres were 4–6 μm , 2.48 eV, and 2.62 m^2/g , respectively. The BiVO_4 microspheres exhibited the highest photocatalytic activity with ca. Ninety-eight percentage degradation of RhB, remarkably superior to the pure monoclinic–scheelite BiVO_4 and tetragonal–zircon BiVO_4 . The enhanced photocatalytic performance was attributed to the more effective separation of photogenerated carriers generated in the heterophasic BiVO_4 . Based on free radical scavenging and N_2/O_2 -purging experiments, the degradation of RhB was believed to be driven mainly by the participation of $\cdot\text{O}_2^-$ and a lesser extent by the participation of holes and $\cdot\text{OH}$.

Sun et al. [31] prepared monoclinic scheelite BiVO_4 hollow spheres (diameter = 3000–4000 nm) using a simple hydrothermal method with urea as guiding surfactant. It is observed that the RhB removal efficiency of BiVO_4 hollow spheres was more than 80% after 50 min of visible-light irradiation without adding any H_2O_2 . The superior activity of the *m*- BiVO_4 sample was attributed to two reasons: (i) the BET surface area of the hierarchical hollow spheres was 10.6 m^2/g , the higher surface area provided not only more surface reached by the visible light but also more active sites, which would result in good photocatalytic performance and (ii) the large hollow space inside the microspheres greatly decreased the density of *m*- BiVO_4 , thus rendering them to be easily suspended in water.

Monoclinic BiVO_4 crystals with a particle size of 400–700 nm and a surface area of 1.75 m^2/g were synthesized with the assistance of cetyltrimethylammonium bromide (CTAB) [2]. The given RhB solution (100 mL, 10^{-5} M) was completely degraded within 20 min of visible-light irradiation, which was due to the addition of CTAB during the catalyst fabrication process.

Many other researchers also reported various kinds of spherical BiVO_4 crystallites (Table 1). For example, Ma et al. [32] prepared BiVO_4 microspheres by a hydrothermal method in the presence of ethylenediamine tetraacetic acid (EDTA) for the removal of MB under sunlight illumination. Jiang et al. [22] reported porous spherical BiVO_4 using urea as pH adjustor and polyvinyl pyrrolidone (PVP) as surfactant for MO degradation. Castillo et al. [33] studied flame-assisted synthesis of nanoscale spherical BiVO_4 for the degradation of MB under visible-light illumination. These spherical BiVO_4 samples exhibited good photocatalytic activities for the degradation of organic dyes under visible-light irradiation.

2.2. Flower-like BiVO_4

A flower-like morphology is usually composed of nanorods or nanosheets. Flower-like particles not only look beautiful, but also show good photocatalytic performance. Fan et al. [34] prepared monoclinic BiVO_4 with a flower-like morphology via a simple hydrothermal route by adjusting the amount of surfactant (PVP K30). The photocatalytic efficiency for the decolorization of MB aqueous solution could reach 75% in 2 h of visible-light irradiation. The UV-visible diffuse reflectance absorption spectra reveal that this BiVO_4 sample showed excellent absorption of visible light in the region of up to 600 nm, and the E_g was 2.14 eV. The flower-like sample was composed of numerous BiVO_4 sub-nanoparticles (400–500 nm)

(Figure 2). The BiVO₄ possessed a small size, a narrow bandgap energy, and a high BET surface area (61.6 m²/g), which facilitated the enhancement of photocatalytic activity.

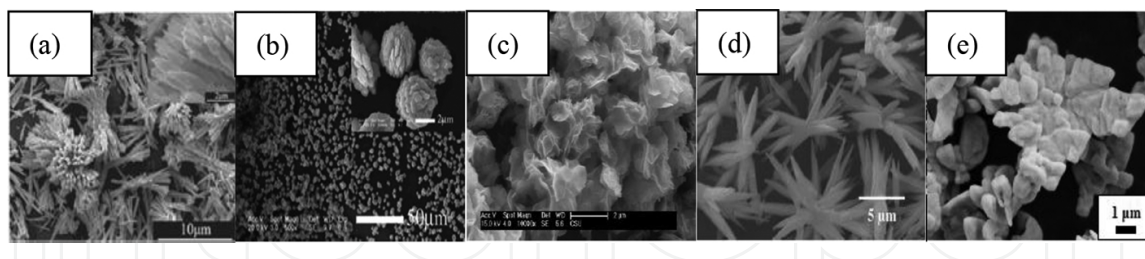


Figure 2. SEM images of flower-like BiVO₄: (a) [28], (b) [34], (c) [36], (d) [37], and (e) [38].

An *m*-BiVO₄ sample with a regular morphology was prepared using a facile hydrothermal method with Bi₂O₃ and NH₄VO₃ as starting material [36]. The as-synthesized sample had a flower-like structure with a diameter of 1–2 μm and a bandgap energy of 2.46 eV. About 58% of MO in the aqueous solution was degraded after sunlight irradiation for 4 h. Photocatalytic performance of the as-prepared BiVO₄ sample was much better than that of P25 under the same reaction conditions, which might be ascribable to the flower structure and the larger surface area of the nanosheet-like BiVO₄ sample. Larger surface area can facilitate the harvesting of light, whereas the thinness of the nanosheets can cause a bigger distortion of the unit cell induced by the large surface strain. All of those factors might contribute to the improvement in photocatalytic activity of BiVO₄.

2.3. Rod-like BiVO₄

Figure 3 shows the scanning electron microscopic (SEM) images of the rod-like BiVO₄ samples. Hu et al. [27] reported the controlled fabrication of monoclinic BiVO₄ with a rod-like structure and investigated the effect of calcination temperature on the sunlight-driven photocatalytic degradation of RhB. It is found that the sample calcined at 300°C exhibited a superior photocatalytic activity: RhB at an initial concentration of RhB lower than 10 mg/L could be completely decolorized after 6 h of sunlight irradiation. The bandgap energy and BET surface area of the rod-like BiVO₄ photocatalyst were 2.46 eV and 3.5 m²/g, respectively. It can be observed from the SEM images (Figure 3) that the sample obtained after calcination at 300°C was composed of dispersive and short rod-like nanocrystals, thus displaying higher BET surface area, which would enhance the adsorption ability and hence improve the photocatalytic performance. Dai and coworkers [35] prepared monoclinic BiVO₄ single crystallites with different morphologies using the triblock copolymer P123-assisted hydrothermal strategy with bismuth nitrate and ammonium metavanadate as metal source and various bases as pH adjustor. The rod-like BiVO₄ sample was obtained at pH = 6 using NH₃-H₂O as pH adjustor. This sample displayed a higher surface area (3.2 m²/g) and a lower bandgap energy (2.26 eV). The rod-like BiVO₄ sample showed excellent visible-light-driven photocatalytic activity for MB degradation in an aqueous solution under visible light irradiation: 90% degradation was achieved within 2 h of reaction. The unusually high visible-light-driven catalytic performance of monoclinically crystallized rod-like BiVO₄ single crystallite was associated with its

higher surface area and surface oxygen defect concentrations as well as the unique particle morphology.

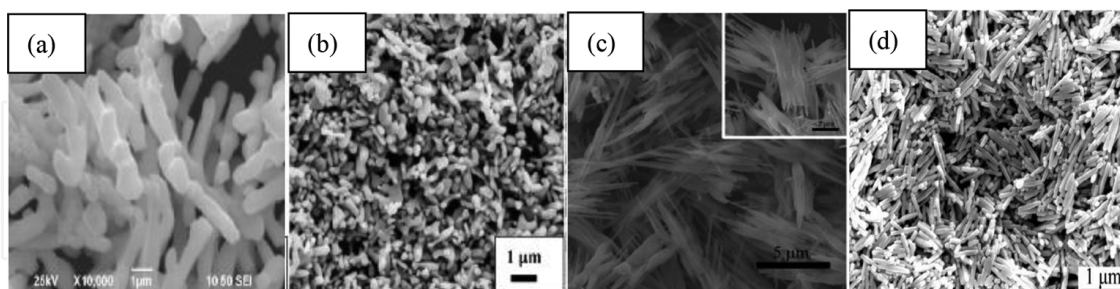


Figure 3. SEM images of rod-like BiVO_4 : (a) [27], (b) [35], (c) [39], and (d) [40].

2.4. Peanut-like BiVO_4

Chen et al. [41] synthesized *m*- BiVO_4 with a hollow peanut-like morphology (**Figure 4b**) using L-lysine as surfactant, and studied its photocatalytic activity for the degradation of crystal violet under solar light irradiation. The best performance was observed over the sample crystallized at 160°C in the presence of L-lysine and after calcination at 550°C . Ninety-eight percentage of the crystal violet could be removed after exposure for 1 h. Although the surface area decreased with the rise in calcination temperature [$2.0 \text{ m}^2/\text{g}$ (at 350°C), $0.86 \text{ m}^2/\text{g}$ (at 450°C), and $0.54 \text{ m}^2/\text{g}$ (at 550°C)], their bandgap energies were about 2.4 eV, and the sample calcined at 550°C performed better than the one calcined at 450 or 350°C . The authors assigned the good photocatalytic activity of *m*- BiVO_4 to its unique hollow peanut-like morphology and pure monoclinic phase of high crystallinity, rather than to the bandgap energy and surface area. The physical properties and photocatalytic activities of several kinds of peanut-like BiVO_4 samples reported in the literature are listed in **Table 1**.

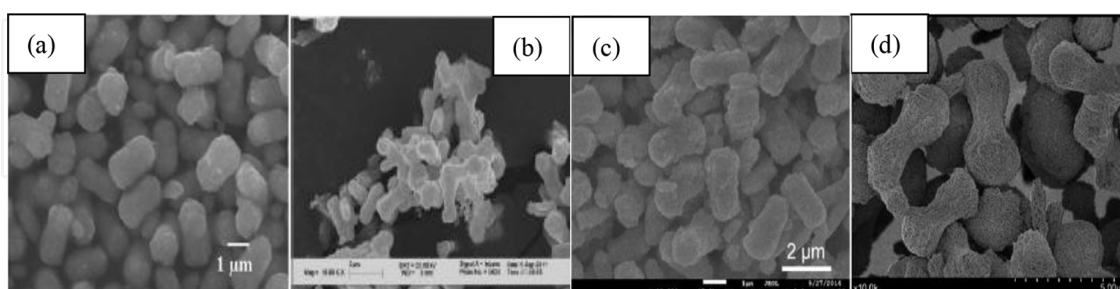


Figure 4. SEM images of peanut-like BiVO_4 : (a) [37], (b) [41], (c) [42], and (d) [43].

2.5. Polyhedron-like BiVO_4

The physical properties and photocatalytic activities of the related polyhedral BiVO_4 samples are summarized in **Table 1**. For example, Han et al. [44] reported the synthesis of

monodispersed octahedral *m*-BiVO₄ nanocrystals via a simple hydrothermal route in the presence of sodium dodecyl benzene sulfonate (SDBS). The octahedral *m*-BiVO₄ nanocrystal with a size of 200–300 nm (**Figure 5b**) exhibited the highest photocatalytic activity (RhB was completely degraded within 10 h of visible-light irradiation). The octahedral crystals displayed higher surface area (3.97 m²/g) and narrower bandgap energy (2.25 eV). Such a good photocatalytic activity was attributed to the good crystallization with fewer structural defects and preferred crystal facets for surface-controlled photocatalysis as well as the better optical absorption property and higher surface area. Zhu et al. [45] has successfully synthesized monoclinic decahedral BiVO₄ by the microwave-assisted hydrothermal method with Tween-80 as template. The photocatalytic efficiency of decahedral BiVO₄ obtained hydrothermally at 160°C showed the highest photocatalytic MB degradation efficiency (ca. 82% MB was degraded after 160 min of visible-light irradiation). The bandgap energy of the sample derived hydrothermally at 160°C was 2.35 eV. The authors concluded that the good photocatalytic performance of the decahedral BiVO₄ sample was related to the imperfect crystal and small size, which resulted in the efficient separation of the electron–hole pairs.

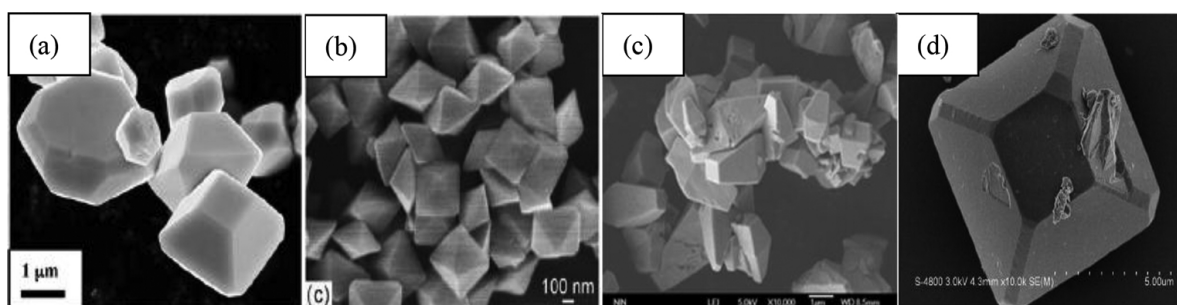


Figure 5. SEM images of polyhedron-like BiVO₄: (a) [35], (b) [44], (c) [45], and (d) [46].

2.6. Olive-like BiVO₄

The physical properties and photocatalytic activities of several kinds of olive-like BiVO₄ samples are listed in Table 1. Adopting the facile pH-dictated solvothermal route with the aid of either NH₃–H₂O or NaOH, Dong et al. [37] controllably synthesized the uniform monoclinic scheelite BiVO₄ with hierarchical structures. As the pH value was adjusted to 6.26 using NaOH as the pH controller, the olive-like BiVO₄ crystallites (bandgap energy = 2.40 eV) was generated. The olive-like BiVO₄ sample showed a RhB degradation efficiency of 97% after 10 h of sunlight irradiation. It should be noted that this sample did not have a high surface area (4.6 m²/g) in comparison with other samples (surface area = 6.3–11.1 m²/g) obtained at different pH values. Apparently, the enhanced photocatalytic performance was not related to the surface area and aspect ratios of the fabricated photocatalysts, but to the unique morphological configurations. Lei et al. [39] synthesized olive-like BiVO₄ using a hydrothermal strategy at pH = 3.0. As seen from the SEM images (**Figure 6c**), the sizes of the BiVO₄ particles were predominantly 1.8–2.9 μm in length and 1.1–1.8 μm in diameter. The olive-like BiVO₄ photocatalyst with a bandgap energy of 2.5 eV showed the highest photocatalytic activity,

which could photocatalytically degrade 50.5% RhB after 150 min of visible-light illumination. The synergic effect of monoclinic phase and particle size contributed to the high photocatalytic efficiency of the olive-like BiVO_4 photocatalyst.

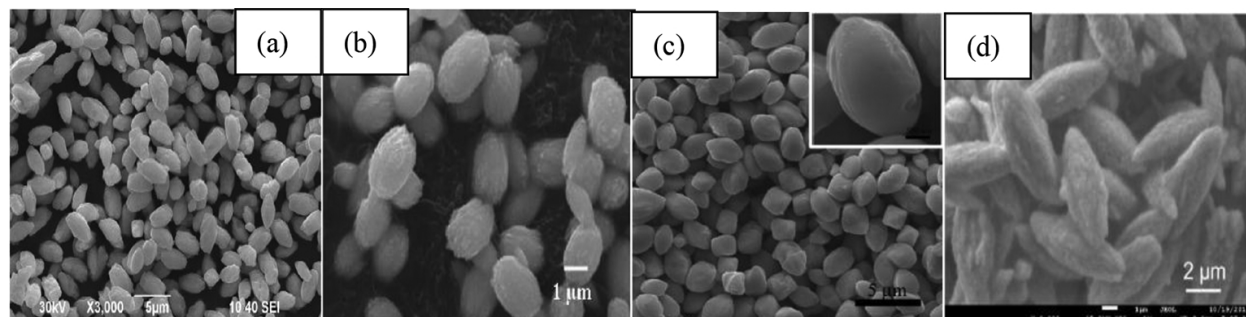


Figure 6. SEM images of olive-like BiVO_4 : (a) [26], (b) [37], (c) [39], and (d) [42].

Dai and coworkers [38] fabricated the BiVO_4 samples with a monoclinic scheelite-type structure and various morphologies via an alcohol-hydrothermal route with $\text{Bi}(\text{NO}_3)_3$ and NH_4VO_3 as precursor and sodium hydroxide as pH adjuster in the absence or presence of triblock copolymer P123. It is realized that the pH of the precursor solution and the surfactant greatly affected the particle shape and architecture of BiVO_4 . Porous BiVO_4 particles with spherical, flower-like, and sheet-like shapes were obtained in the presence of P123 at a reaction temperature of 180°C and a pH of 2, 7, or 10, respectively. A rod-like BiVO_4 was generated at reaction temperature = 180°C and pH = 2. The four BiVO_4 samples possessed a surface area of 1.4–3.8 m^2/g and a bandgap energy of 2.47–2.54 eV. The difference in morphology of the BiVO_4 particles gave rise to discrepancies in surface area, surface oxygen deficiency density, and (040) crystal face exposure. The rod-like BiVO_4 sample that possessed the largest surface area, the highest surface oxygen deficiency density, the highest (040) crystal face exposure, and the lowest bandgap energy performed the best for MO degradation under visible-light irradiation. It is concluded that the particle morphology could influence the photocatalytic activity of BiVO_4 and the rod-like shape was favorable for the improvement in photocatalytic activity.

2.7. Microtube-like BiVO_4

The physical properties and photocatalytic activities of tubular BiVO_4 samples reported in the literature are summarized in **Table 1**. Single-crystalline monoclinic BiVO_4 microtubes with a side length of 800 nm and a wall thickness of 100 nm (**Figure 7b**) were synthesized by a facile reflux method at 80°C [47]. The results of optical absorption experiments reveal that in addition to the UV light region, the BiVO_4 microtubes also had a strong absorption in the visible-light region and the bandgap energy was estimated to be 2.36 eV. The RhB photodegradation over the BiVO_4 microtubes was up to 96% after 3 h of visible-light irradiation, which could be associated with its distinctive morphology.

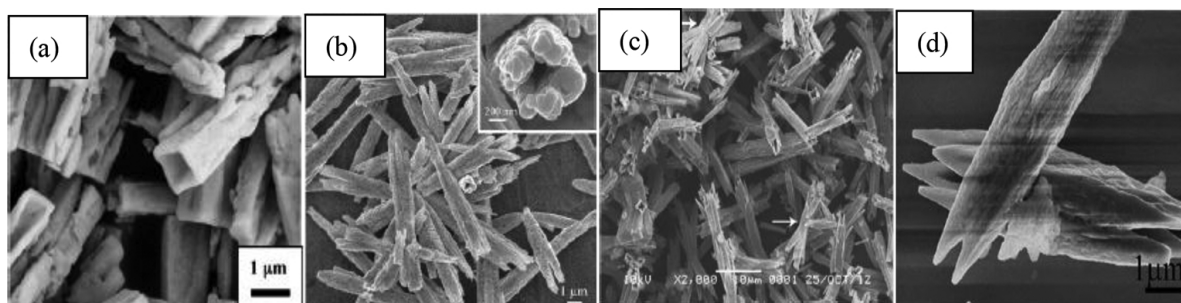


Figure 7. SEM images of microtube-like BiVO₄: (a) [35], (b) [47], (c) [48], and (d) [49].

2.8. Dumbbell-like BiVO₄

Lu et al. [50] reported the controllable synthesis of dumbbell-like BiVO₄ with a hierarchical nanostructure (**Figure 8b**) and a bandgap energy of 2.51 eV by employing a simple hydrothermal process. The photocatalytic degradation of RhB over the dumbbell-like BiVO₄ sample was up to 90% within 4.5 h of visible-light irradiation, which was much higher than the P25 sample under the same reaction conditions. The good visible-light-driven photocatalytic efficiency was related to the exposed crystal planes, which could not only provide more active sites for the photocatalytic reaction but also effectively promote the separation efficiency of the electron-hole pairs. The physical properties and photocatalytic activities of several kinds of dumbbell-like BiVO₄ samples reported in the literature are summarized in **Table 1**.

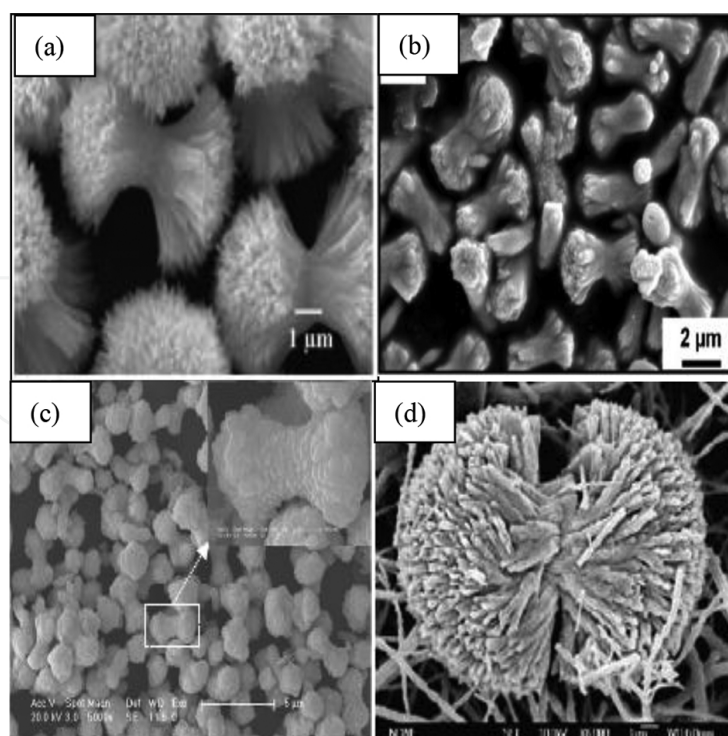


Figure 8. SEM images of dumbbell-like BiVO₄: (a) [37], (b) [50], (c) [51], and (d) [52].

2.9. Needle-like BiVO₄

The physical properties and photocatalytic activities of the typical needle-like BiVO₄ samples are summarized in **Table 1**. For example, Obregón et al. [43] prepared monoclinic BiVO₄ with different morphologies by a surfactant-free hydrothermal method through adjusting the pH value, precipitating agent type, hydrothermal temperature, and treatment time. The needle-like particles (**Figure 9b**) obtained with hydrothermal treatment at 100°C and NH₄OH as pH controlling agent showed the best efficiency (50–60% after 2 h of UV-visible-light irradiation) for MB photodegradation. The surface areas of the samples obtained with hydrothermal treatment time of 2, 8, and 20 h were 30.2, 2.7, and 1.6 m²/g, respectively. It should be noted that the slight diminution in surface area had no clear effect on the photocatalytic performance of the sample. Therefore, the best performance was not associated with the surface area, but strongly affected by the crystallite size and morphology.

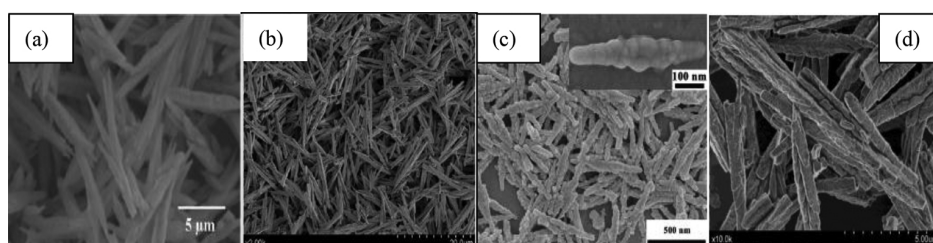


Figure 9. SEM images of needle-like BiVO₄: (a) [37], (b) [43], (c) [53], and (d) [54].

2.10. BiVO₄ with other morphologies

In addition to the well-morphological BiVO₄ samples described above, there are some kinds of BiVO₄ samples with other morphologies (**Figure 10**) that have been prepared. Most of them perform well in the photocatalytic degradation of organic dyes (**Table 1**).

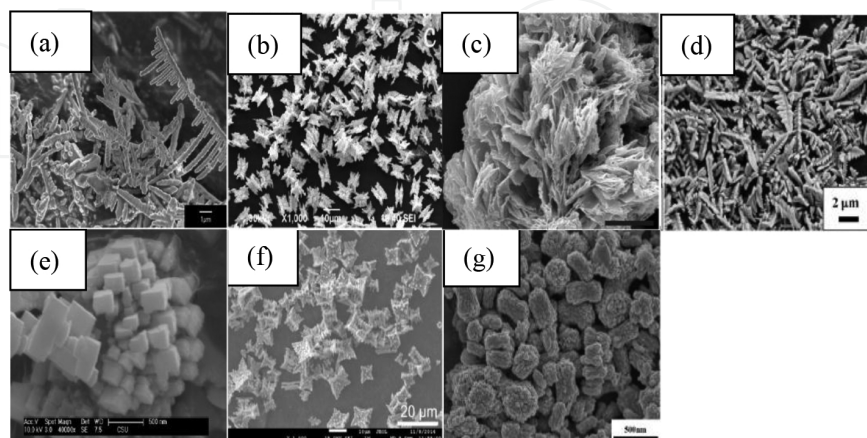


Figure 10. SEM images of BiVO₄ with various morphologies: (a) [16], (b) [26], (c) [31], (d) [35], (e) [36], (f) [42], and (g) [53].

3. Porous BiVO₄ photocatalysts

Most of the monoclinic BiVO₄ samples obtained using the above methods are bulk materials and are low in surface area (<4 m²/g) [55, 56], which is unfavorable for photocatalytic applications. The reasons are as follows: (i) the amount of surface active sites is intimately related to the surface area [57, 58] and (ii) a porous architecture can increase the ability to capture incident light and the transfer of reactant and product molecules [59]. Therefore, it is of significance to controllably prepare BiVO₄ photocatalysts that are porous in structure and high in surface area. The physical properties and photocatalytic activities of typical porous BiVO₄ samples are summarized in **Table 2**.

Photocatalyst	Crystal structure	Crystallite size (nm)	Surface area (m ² /g)	E _g (eV)	Reaction condition	Degradation efficiency and light illumination time	References
3DOM BiVO ₄	Monoclinic	185	23.6	2.50	Visible light, 200 mL phenol (0.1 mmol/L), 0.2 g sample	94% and 3 h	[3]
Mesoporous BiVO ₄	Monoclinic	–	8.4	2.45	Visible light, 200 mL MO (0.01 mmol/L), 0.1 g sample	84% and 2 h	[22]
Ordered mesoporous BiVO ₄	Monoclinic	3.5	59	2.20	Visible light, 80 mL MB (10 ppm), 0.08 g sample	85% and 3h	[57]
Mesoporous BiVO ₄	Monoclinic	–	11.8	2.38	Visible light, 200 mL phenol (0.2 mmol/L), 0.2 g sample	91% and 4 h	[60]
Mesoporous BiVO ₄	Monoclinic	2.2	7.2	2.38	Sunlight, 200 mL RhB (0.02 mmol/L), 0.2 g sample	100% and 1 h	[61]
3DOM InVO ₄	Monoclinic	130–140	52.3	2.50	Visible light, 100 mL MB (10 mg/L), 0.1 g sample	98% and 1 h	[62]
15 wt% CrO ₂ /InVO ₄	Monoclinic	155–165	45	2.10	Visible light, 100 mL RhB (15 mg/L), 0.1 g sample	99% and 200 min	[63]
0.08 wt% Au/3DOM InVO ₄ –BiVO ₄	Monoclinic	22.3	25.1	2.54	Visible light, 100 mL RhB (15 mg/L), 0.1 g sample	100% and 50 min	[64]
0.08 wt% Au/3DOM InVO ₄ –BiVO ₄	Monoclinic	22.3	25.1	2.54	Visible light, 100 mL MB (20 mg/L), 0.1 g sample	100% and 90 min	[64]
0.08 wt% Au/3DOM InVO ₄ –BiVO ₄	Monoclinic	22.3	25.1	2.54	Visible light, 100 mL RhB (15 mg/L) + MB (20 mg/L), 0.1 g sample	100% and 120 min	[64]
0.17 wt% Pd/10 wt % AgBr/BiVO ₄	Monoclinic	29.8	12.9	2.49	Visible light, 100 mL 4-chlorophenol (15 mg/L), 0.05 g sample	100% and 2.5 h	[65]

Table 2. Physical properties and photocatalytic activities of the porous BiVO₄ photocatalysts.

By adopting an alcohol-hydrothermal method with $\text{Bi}(\text{NO}_3)_3$ and NH_4VO_3 as precursor, sodium hydroxide as pH adjustor, ethanol and ethylene glycol as solvent, and dodecylamine, oleylamine, or oleic acid as surfactant, Dai and coworkers [59] prepared the BiVO_4 materials with various shapes and/or mesoporous architectures. Photocatalytic activities of the as-derived samples were measured for phenol degradation in the presence of H_2O_2 under visible-light illumination, and effect of phenol concentration on photocatalytic performance was also probed. The authors pointed out that the surfactant and pH exerted a significant impact on particle morphology and crystal phase structure of BiVO_4 . Monoclinic BiVO_4 samples with a porous olive-like shape could be fabricated with dodecylamine, oleylamine, or oleic acid as surfactant at a pH of 1.5 or 3.0 and a reaction temperature of 100°C . Short-rod-like monoclinic BiVO_4 and porous sheet-layered spherical orthorhombic $\text{Bi}_4\text{V}_2\text{O}_{11}$ were generated with dodecylamine as surfactant at reaction temperature = 100°C and pH = 7.0 and 11.0, respectively. Among all of the as-prepared BiVO_4 samples, the porous sample with an olive-like morphology and a surface area of $12.7 \text{ m}^2/\text{g}$ (derived with dodecylamine and at pH = 1.5) exhibited the best visible-light-driven photocatalytic performance for phenol degradation (96% phenol was removed within 4 h of visible-light illumination).

Jiang et al. [60] prepared monoclinic BiVO_4 single crystallites with a porous octapod-like morphology using the P123-assisted hydrothermal method with bismuth nitrate and ammonium metavanadate as metal source and various bases as pH adjustor. The BiVO_4 with a surface area of $11.8 \text{ m}^2/\text{g}$ and a bandgap energy of 2.38 eV showed excellent photocatalytic activities for the degradation of MB and phenol. Near 100 and 91% degradation of MB and phenol were achieved within 2 and 4 h of visible-light irradiation, respectively. The authors concluded that the high visible-light-driven catalytic performance of the porous octapod-like BiVO_4 single crystallites was associated with the higher surface area, porous structure, and lower bandgap energy.

Peanut-shaped porous monoclinic BiVO_4 with high yield was prepared using a simple template-free solvothermal method [61]. The pore size of the sample was 2.2 nm. Compared to the BiVO_4 sample obtained hydrothermally, the porous BiVO_4 sample exhibited a higher photocatalytic activity for the degradation of RhB and maintained high catalytic efficiency in the repeated recycles of the H_2O_2 -containing system. Nearly, complete degradation of RhB was observed after 1 h of sunlight irradiation. It is noteworthy that the bandgap energy (2.38 eV) of the porous BiVO_4 sample was higher than that (2.28 eV) of the nonporous BiVO_4 sample, but the surface area ($7.3 \text{ m}^2/\text{g}$) of the former was considerably higher than that ($2.1 \text{ m}^2/\text{g}$) of the latter.

Li et al. [57] prepared ordered mesoporous monoclinic BiVO_4 using mesoporous silica (KIT-6) as template. The mesoporous BiVO_4 sample had a surface area of $59 \text{ m}^2/\text{g}$ and a pore size of 3.5 nm. The mesoporous BiVO_4 exhibited a superior visible-light-driven photocatalytic activity for the degradation of MB. The degradation rate over the mesoporous BiVO_4 sample was twice as active as the conventional BiVO_4 sample, and 85% MB could be degraded after 3 h of visible-light illumination. The mesoporous BiVO_4 sample possessed a large surface area, an ordered structure, and a small crystal size, thus resulting in excellent visible-light photocatalytic

activity. The most attractive feature of the mesoporous BiVO₄ semiconductor with a bandgap energy of 2.20 eV was its excellent visible-light response ability.

Liu et al. [3] prepared three-dimensionally ordered macroporous (3DOM) bismuth vanadates with a monoclinic crystal structure and high surface areas (18–24 m²/g) using ascorbic acid-assisted poly(methyl methacrylate) (PMMA)-templating strategy. The average macropore size and wall thicknesses of the BiVO₄ samples were in the ranges of 160–185 and 24–70 nm, respectively. The photocatalytic performance of the porous BiVO₄ samples was evaluated for the degradation of phenol in the presence of a small amount of H₂O₂ under visible-light illumination. The results showed that the conversion of phenol could reach 94% at an initial phenol concentration of 0.1 mmol/L after 3 h of visible-light irradiation. However, only 51% phenol was degraded over the bulk BiVO₄ sample. The authors concluded that the excellent photocatalytic activity of 3DOM BiVO₄ was associated with the high-quality 3DOM-structured BiVO₄ that has a high surface area and a surface oxygen vacancy density.

Wang et al. [62] reported the 3DOM-structured monoclinic InVO₄ with high surface areas (35–52 m²/g) using the citric acid-, tartaric acid-, or ascorbic acid-assisted PMMA-templating strategy. From the SEM images, among the as-obtained samples, the InVO₄ sample derived with PMMA in the presence of ascorbic acid showed the best quality in 3DOM architecture and a bandgap energy of 2.50 eV, with the macropore and nanovoid (on the skeletons) sizes being in the ranges of 130–160 and of 2–10 nm, respectively. Ninety-eight percentage MB was removed over the ascorbic acid-derived sample within 1 h of visible-light illumination. It is concluded that the excellent photocatalytic activity of this sample was related to its higher surface area and surface oxygen vacancy density and lower bandgap energy as well as the better quality of 3DOM structure.

Dai and coworker [63] loaded certain amounts of chromia on the surface of 3DOM InVO₄ to obtain the *y*CrO_{*x*}/3DOM InVO₄ (*y* = 5, 10, 15, and 20 wt%) photocatalysts. They investigated the photocatalytic degradation of RhB in the presence of H₂O₂ under visible-light illumination and found that (i) chromia in the *y*CrO_{*x*}/3DOM InVO₄ samples were highly dispersed on the surface of 3DOM InVO₄; (ii) after loading of CrO_{*x*}, the surface areas of the *y*CrO_{*x*}/3DOM InVO₄ samples decreased; (iii) after visible-light illumination for 200 min, the RhB conversion was 47% over 3DOM InVO₄, 90% over 5CrO_{*x*}/3DOM InVO₄, 96% over 10CrO_{*x*}/3DOM InVO₄, 97% over 20CrO_{*x*}/3DOM InVO₄, and 99% over 15CrO_{*x*}/3DOM InVO₄; (iii) the *y*CrO_{*x*}/3DOM InVO₄ samples exhibited stronger absorption in the UV- and visible-light than the 3DOM InVO₄; (iv) the *y*CrO_{*x*}/3DOM InVO₄ samples possessed higher amounts of surface oxygen vacancies than the 3DOM InVO₄ sample. These authors concluded that the good visible-light-driven catalytic activity of 15CrO_{*x*}/3DOM InVO₄ was associated with its CrO_{*x*} loading, higher surface area and surface oxygen vacancy density, and lower bandgap energy as well as the better quality of 3DOM structure.

Ji et al. [64] prepared the 3DOM InVO₄-BiVO₄ (InBi-3D) and its supported noble metal (*M*) nanoparticles (0.17 wt% *M*/InBi-3D, *M* = Au, Ag, Pd, Pt) using the PMMA-templating and polyvinyl alcohol (PVA)- or PVP-assisted reduction methods, respectively. There was co-presence of orthorhombic InVO₄ and monoclinic BiVO₄ in the InBi-3D or *M*/InBi-3D samples. The as-fabricated samples displayed a surface area of 17–30 m²/g, a *M* particle size of 2.5–3.8

nm, and a bandgap energy of 2.50–2.56 eV. The 0.08 wt% Au/InBi-3D sample exhibited the best photocatalytic activity: The complete degradation of RhB, MB, and RhB + MB could be achieved within 50, 90, and 120 min of visible-light illumination. The authors believe that the 3DOM hierarchical architecture, InVO₄–BiVO₄ composite, and high dispersion of plasmonic gold nanoparticles were the main factors responsible for excellent photocatalytic efficiency of the InBi-3D-supported Au sample.

Dai and coworkers [65] prepared 3DOM BiVO₄ (3D-BiV), AgBr/3D-BiV, and M/AgBr/3D-BiV (*M* = Au, Pt, and Pd) photocatalysts using the PMMA-templating, low-temperature deposition, and PVA-protected reduction methods, respectively. The AgBr and noble metals were uniformly distributed on the surface of 3D-BiV. The 3DOM BiVO₄ sample performed better than the commercial TiO₂ sample. The 10 wt% AgBr/3D-BiV sample exhibited a reduced performance, which might be caused by the shielding effect of excessive AgBr in visible-light spectrum on the 3DOM BiVO₄ support. When noble metal was deposited on the surface of 10 wt% AgBr/3D-BiV, the photocatalytic performance was much improved, and the 0.17 wt% Pd/AgBr/3D-BiV sample performed the best: Almost complete degradation of 4-chlorophenol was achieved within 150 min of visible-light illumination. The authors assigned the excellent photocatalytic performance of 0.17 wt% Pd/AgBr/3D-BiV to the good 3DOM structure, high surface oxygen adspecies concentration, easy transfer and separation of photogenerated carriers, and synergistic effect between AgBr or Pd nanoclusters and BiVO₄.

4. Heteroatom-doped BiVO₄ photocatalysts

Up to now, many investigations have been made to improve the photocatalytic performance of visible-light-responsive BiVO₄ by doping heteroatoms that can efficiently avoid the charge recombination via trapping both electrons and holes. The co-doping with both cations and anions can also extend the visible-light absorption spectrum of BiVO₄.

4.1. Doping with anions

Yin et al. [66] reported the one-step fabrication of high-performance C-doped BiVO₄ photocatalyst with hierarchical structures under visible-light irradiation. The sample calcined at 400°C with a carbon content of 1.5 wt% showed the best photocatalytic MB degradation efficiency (100% degradation after 1 h of visible-light irradiation), which was 6.3 times higher than that over the pure BiVO₄ sample (18% degradation after 1 h of visible-light irradiation). The XRD result showed that 1.5 wt% C-BiVO₄ had a smaller crystalline size (18.7 nm) in comparison with pure BiVO₄ (28.5 nm). Moreover, the bandgap energy of 1.5 wt% C-BiVO₄ was about 2.39 eV, which was smaller than that (2.46 eV) of pure BiVO₄. The photocatalytic performance was enhanced by C-doping because it improved the efficient separation and transfer of the photogenerated electrons and holes, as evidenced by the results of electron paramagnetic resonance (EPR) measurements.

Tan et al. [67] fabricated a N-doped monoclinic BiVO₄ photocatalyst via a facile microwave hydrothermal route using NaN₃ as nitrogen source. The photocatalytic performance of the samples was evaluated by the decolorization of RhB under the simulated sunlight irradiation. After 4 h of the simulated sunlight irradiation, the degradation efficiencies over the pure BiVO₄ and N-doped BiVO₄ samples were 48 and 97%, respectively, indicating that N-doped BiVO₄ was twice as active as pure BiVO₄. The bandgap energy (2.0 eV) of N-doped BiVO₄ was narrower than that (2.2 eV) of pure BiVO₄, whereas the surface area (1.34 m²/g) of the former was close to that (0.21 m²/g) of the latter. The enhancement in photocatalytic activity could be attributable to the small particle size, narrow bandgap, and most importantly, the existence of multi-atomic BiVO₄ centers and surface oxygen vacancies, which improved the mobility of charge carriers and inhibited the recombination of charge carriers.

F-doped BiVO₄ particles were synthesized through a simple two-step hydrothermal process [68]. The XRD results demonstrated that the presence of F⁻ ions did not change the phase structure of monoclinic BiVO₄. F-doped BiVO₄ was consisted of relatively uniform spheres with a diameter of 2–4 μm, and the bandgap energy was 2.39 eV. When the BiVO₄/NaF molar ratio was 1: 0.9, the derived F-doped BiVO₄ sample exhibited the highest photocatalytic MB degradation activity (99% MB was degraded after 3 h of visible-light irradiation). The appropriate amount of F⁻ ions introduced into the BiVO₄ crystal lattice might effectively restrain the recombination of photogenerated electron–hole pairs, thus facilitating the improvement in photocatalytic activity.

Jiang et al. [69] prepared fluoride-doped BiVO₄ with the different F/Bi molar ratios using the hydrothermal strategy with the hydrothermally derived BiVO₄ as precursor and NH₄F as fluoride source. All of the samples were of single-phase monoclinic scheelite structure. The doping of fluorine did not induce any alteration in crystal structure but changed the morphology of the sample particles. Compared to the undoped BiVO₄ sample, the fluoride-doped BiVO₄ samples showed higher oxygen adspecies concentration. When the F/Bi molar ratio was 0.29, the BiVO₄ sample with a surface area of 14.6 m²/g and a bandgap energy of 2.42 eV performed the best for the degradation of phenol, giving a 97% phenol degradation efficiency within 2 h of visible-light irradiation. The authors concluded that the excellent photocatalytic performance of fluoride-doped BiVO₄ was associated with its higher surface area and adsorbed oxygen species concentration, stronger optical absorbance performance, and lower bandgap energy.

Other anions (e.g., S and B) were also doped into the BiVO₄ lattice (**Table 3**). For example, Guo et al. [70] found that S-doped BiVO₄ was superior to pure BiVO₄ in photocatalyzing the degradation of MB under visible-light irradiation, since an appropriate amount of S²⁻ ions could improve the separation efficiency of photogenerated electron–hole pairs and hinder their recombination.

Photocatalyst	Crystal structure	Crystallite size (nm)	Surface area (m ² /g)	E _g (eV)	Reaction condition	Degradation efficiency and light illumination time	References
0.5 wt% C-BiVO ₄	Monoclinic	35.7	1.18	-	Visible light, 200 mL phenol (5 mg/L), 0.2 g sample	88.7% and 5 h	[79]
4 mol% B-BiVO ₄	Monoclinic	23.0	4.17	2.34	Visible light, 50 mL MO (15 mg/L), 0.01 g sample	96% and 50 min	[80]
F-BiVO ₄ (F/Bi molar ratio = 0.29)	Monoclinic	-	14.6	2.42	Visible light, 200 mL phenol (0.2 mmol/L), 0.2 g sample	97% and 2 h	[69]
0.17 wt% S-BiVO ₄	Monoclinic	29.01	3.18	2.44	Visible light, 100 mL MB (10 mg/L), 0.1 g sample	100% and 25 min	[70]
0.08 wt% S-BiVO ₄	Monoclinic	-	9.9	2.40	Visible light, 100 mL MB (0.005 mmol/L), 0.01 g sample	95% and 2 h	[71]
1.40 wt% FeO _x /BiVO _{4-δ} S _{0.08}	Monoclinic	-	5.1	2.39	Visible light, 100 mL MB (0.01 mmol/L), 0.01 g sample	100% and 90 min	[72]
N-BiVO ₄ (N : Bi molar ratio = 0.2)	Monoclinic	49.8	3.03	2.23	Visible light, 50 mL MO (10 mg/L), 0.01 g sample	85% and 50 min	[81]
1% wt% Cu-BiVO ₄	Monoclinic	39.78	15.37	1.90	UV light, 90 mL MB (5096 mg/L), 0.15 g sample	and 2 h	[82]
2 mol% Mo-BiVO ₄	Monoclinic	-	0.1	2.39	Visible light, MB (16 ppm), 0.1 g sample	100% and 1.5 h	[78]
1.08 wt% Er-BiVO ₄	Monoclinic	-	4.39	2.11	Visible light, 100 mL MO (10 mg/L), 0.2 g sample	99.4% and 3 h	[83]
8 mol% Yb-BiVO ₄	Tetragonal	-	11.02	2.9	Sunlight, 50 mL RhB (5 mg/L), 0.05 g sample	98% and 2 h	[84]
3 mol% Yb/0.75 mol % Er-BiVO ₄	Monoclinic/ tetragonal	-	4	2.35/2.68	UV-vis-NIR light, 150 mL MB (10 ppm), 1 g/L sample	100% and 1 h	[77]
0.8 wt% Eu/4 wt% B-BiVO ₄	Monoclinic	44.89	4.61	2.28	Visible light, 50 mL MO (15 mg/L), 0.015 g sample	90% and 50 min	[76]

Table 3. Physical properties and photocatalytic activities of the heteroatom-doped BiVO₄ photocatalysts.

Employing a dodecylamine-assisted alcohol-hydrothermal method in the absence and presence of thiourea or Na₂S, Zhao et al. [71] synthesized the sulfur-doped BiVO₄ samples. The S-doped samples possessed a monoclinic scheelite structure and a surface area of 8.4–9.9 m²/g, and the bandgap energies of the S-doped BiVO₄ samples were narrower than that of pure BiVO₄. The S-doped BiVO₄ sample with a S content of 0.78 wt% showed the best photocatalytic performance for the degradation of MB and formaldehyde. The photodegradation efficiency of MB was 92% within 2.5 h of visible-light illumination, but only 45% MB was degraded over pure BiVO₄ under the same conditions. It is believed that a higher adsorbed oxygen species concentration and a lower bandgap energy were responsible for the excellent photocatalytic activity of the 0.78 wt% S-BiVO₄ sample. These authors also investigated the porous olive-like morphological S-doped bismuth vanadate-supported iron oxide (γ FeO_x/BiVO₄S_{0.08}, $y = 0.06$ – 1.40 wt%) photocatalysts derived from the dodecylamine-assisted alcohol-hydrothermal and incipient wetness impregnation methods [72]. It is shown that the γ FeO_x/BiVO₄S_{0.08} photocatalysts possessed a monoclinic scheelite BiVO₄ phase, a porous olive-like shape, a surface area of 8.8–9.2 m²/g, and a bandgap energy of 2.38–2.42 eV. Bi⁵⁺, Bi³⁺, V⁵⁺, V³⁺, Fe³⁺, and Fe²⁺ species were concurrently present on the surface of γ FeO_x/BiVO₄S_{0.08}. Among all of the as-fabricated samples, the 1.40 wt% FeO_x/BiVO₄S_{0.08} sample showed the highest photocatalytic activity for MB degradation under visible-light irradiation. It is concluded that the sulfur and FeO_x co-doping, higher adsorbed oxygen species concentration, and lower bandgap energy were responsible for the excellent visible-light-driven catalytic activity of 1.40 wt% FeO_x/BiVO₄S_{0.08}.

4.2. Doping with cations

Cation doping is another approach to enhance the photocatalytic degradation efficiency of BiVO₄, including transition metal doping and rare-earth doping (Table 3). For example, Li et al. [73] prepared Cu-doped monoclinic BiVO₄ by a facile hydrothermal method and used the degradation of RhB to evaluate their photocatalytic activities. 1 wt% Cu-BiVO₄ showed the best degradation performance: 95% of RhB was degraded within 80 min of visible-light irradiation, whereas pure BiVO₄ can only degrade 60% of RhB within the same time. The bandgap energy of 1 wt% Cu-BiVO₄ was 2.55 eV, resulting in the photoabsorption ability of the 1 wt% Cu-BiVO₄ sample slightly stronger than undoped BiVO₄ (bandgap energy = 2.57 eV). The amount of oxygen vacancies increased in the copper-doped samples. Possible factors that significantly enhance photocatalytic performance could be as follows: (i) Cu²⁺ substituted partial V⁵⁺ ions with lower oxidation state, generating a certain amount of oxygen vacancies; (ii) the generated oxygen vacancies can capture the electrons to suppress recombination of the photoinduced carriers; and (iii) the photoinduced carriers freely diffuse to the active sites on the surface of the photocatalyst where oxidation of organic species takes place.

Zhou et al. [74] prepared a series of visible-light-sensitive monoclinic Co-BiVO₄ photocatalysts by the heteronuclear complexing method with diethylenetriamine pentaacetic acid (DTPA) as chelating agent. The bandgap was narrowed by doping cobalt. The bandgap energies of the Co-doped BiVO₄ samples at cobalt molar content of 0 and 1–10 wt% were 2.44 and 2.39–2.43 eV, respectively. The photocatalytic activity of Co-BiVO₄ was studied by the

decolorization of MB. The 5 wt% Co-BiVO₄ sample exhibited the highest photocatalytic activity with a 85% of MB removal (65% of MB removal by pure BiVO₄) within 5 h of visible-light irradiation. There was no significant loss of photocatalytic activity in three successive runs (each lasted for 6 h). Therefore, Co-BiVO₄ was photocatalytically stable and resistant to photocorrosion during the photocatalytic degradation of organic dyes.

Obregón et al. [75] synthesized Er-BiVO₄ by means of a microwave-assisted hydrothermal method and examined the photodegradation of MB under sunlike excitation. The Er-doped BiVO₄ sample showed a mixed phase of monoclinic and tetragonal structures. The optimal MB conversion was achieved over the sample with 0.75 atom% of erbium, over which the complete MB degradation was reached after 40 min of light illumination. The reaction rate obtained over this photocatalyst was 20 times higher than that over the undoped BiVO₄ sample. Two clear absorption edges in the diffuse reflectance spectra of the sample appeared, and the corresponding bandgap energies were ca. 2.4 and 2.8 eV, which were associated with the monoclinic and tetragonal phases, respectively. In order to understand the role of erbium doping in the luminescent properties of the sample, the photoluminescence spectra upon 523 and 655 nm excitations were studied. Upon 655 nm excitation, the up-converted emission of the 0.75 atom% Er-BiVO₄ sample was almost suppressed in the 400–600 nm range. Therefore, the dramatic improvement in photocatalytic activity induced by Er³⁺ doping could correlate to a co-operative process involving the electronic and luminescence mechanism. This sensitization mechanism could improve the photon efficiency of the photocatalytic process, and the formation of a monoclinic–tetragonal heterostructure could also be responsible for a more effective charge separation.

Co-doping with two different elements can exhibit better photocatalytic activity than the doping of single element. Wang et al. [76] reported that photodegradation of MO over BiVO₄ doped with B species showed a higher MO degradation rate than the pure BiVO₄ sample under visible-light irradiation. With the doping of europium, the photocatalytic MO degradation rate over Eu–B co-doped BiVO₄ increased with the rise in europium content, and then decreased when the amount of europium was high enough. Co-doping of two different elements can further increase the photocatalytic activity due to the synergistic effects of a number of factors (such as higher specific area, smaller E_g , and more oxygen vacancies) induced by the co-doping of Eu and B.

Obregón et al. [77] also reported a highly active monoclinic–tetragonal BiVO₄ by doping with Yb³⁺ and Er³⁺, which can completely photodegrade MB within 1 h of sunlike excitation. According to the results of structural and morphological characterization, one can deduce that the presence of Yb³⁺ and Er³⁺ induced the stabilization of the tetragonal phase probably due to its partial incorporation into the BiVO₄ lattice. The improved photocatalytic efficiency was ascribed to two reasons: (i) the doping of lanthanide ions favored the co-existence of a monoclinic-tetragonal heterostructure, and such a structural configuration could optimize the charge separation and (ii) Yb³⁺ and Er³⁺ luminescence tandem led to a supportive photoluminescence up-conversion process, which could render the energy transfer process from erbium ions to the monoclinic BiVO₄ phase.

It should be noted that not all of the photocatalytic activity enhancement can be ascribed to the higher specific area, small crystallite sizes, smaller E_g , and more oxygen vacancies of the heteroatom-doped BiVO₄ samples. For example, Yao et al. [78] reported that the doping of Mo ions could significantly enhance the photocatalytic activity of BiVO₄ for MB photodegradation, which was due to its strong acidity on the surface instead of the reasons mentioned above. Moreover, many other researchers also studied the effect of heteroatom-doping on photocatalytic activity of BiVO₄, as been summarized in Table 3.

5. BiVO₄-based heterojunction photocatalysts

In comparison with single-component photocatalyst, the heterostructure photocatalyst usually exhibits a higher photocatalytic performance for the degradation of various organic contaminants since it can facilitate the effective separation of photoinduced carriers and suppress the recombination of the electron-hole pairs, leaving more charge carriers to form reactive species [85].

Absorption of photons by a semiconductor photocatalyst induces the photogenerated electrons and holes. The photogenerated charge carriers are separated or recombined on the way to the surface reaction sites. The charge separation is a crucial factor determining the light to conversion efficiency [9]. Therefore, much attention has been paid on increasing the charge separation efficiency. Fabrication of a heterojunction structure has been recognized as a useful strategy to avoid charge recombination in a semiconductor catalyst.

5.1. Co₃O₄/BiVO₄ heterojunction

Co₃O₄ is a *p*-type semiconductor with interesting electronic and magnetic properties, thus various kinds of Co₃O₄/BiVO₄ composite structures have been studied [86]. The enhancement in photocatalytic activity of the Co₃O₄/BiVO₄ composite is attributed to the efficient charge transfer and separation between Co₃O₄ and BiVO₄ driven by the internal electric field or potential difference created by the heterojunction.

Long et al. [86] prepared the Co₃O₄/BiVO₄ composite photocatalyst with a *p-n* heterojunction semiconductor structure using the impregnation method. These authors observed that the Co₃O₄/BiVO₄ composite sample (0.8 wt% cobalt content) obtained after calcination at 300°C showed a much better photocatalytic activity than pure BiVO₄ for phenol degradation under visible-light irradiation. The decrease of phenol concentration over pure BiVO₄ was only about 6% within 3 h of visible-light irradiation, but phenol concentration dropped by 85% after Co₃O₄ was loaded on the surface of BiVO₄ under the same conditions. The enhanced activity was attributed to the formation of a *p-n* heterojunction structure and the decrease of recombination of photogenerated hole-electron pairs.

Yu and coworkers [87] also investigated the BiVO₄ decorated with Co₃O₄, which showed a much higher photocatalytic activity than pure BiVO₄. The authors believed that the high crystallinity of BiVO₄ and the formed *p-n* heterojunction of Co₃O₄/BiVO₄ improved the

photocatalytic performance. The physical properties and photocatalytic activities of the $\text{Co}_3\text{O}_4/\text{BiVO}_4$ heterojunction samples reported in the literature are summarized in **Table 4**.

Photocatalyst	Surface area (m^2/g)	E_g (eV)	Reaction condition	Degradation efficiency and light illumination time	References
0.8 wt% $\text{Co}_3\text{O}_4/\text{BiVO}_4$	1.38	–	Visible light, phenol (18 mg/L), 3 g/L sample	96% and 3 h	[86]
3 wt% $\text{Co}_3\text{O}_4/\text{BiVO}_4$	8.03	2.34	Visible light, 80 mL acid orange II (20 mg/L), 0.05 g sample	78% and 5 h	[87]
9 wt% $\text{BiVO}_4/\text{TiO}_2$	107.7	–	Visible light, 80 mL RhB (0.01 mmol/L), 0.08 g sample	79% and 6 h	[119]
8 mol% $\text{BiVO}_4/\text{TiO}_2$	17	2.4	Visible light, 50 mL RhB (1 mmol/L), 0.02 g sample	95% and 2 h	[120]
40 mol% $\text{CeO}_2/\text{BiVO}_4$	–	2.40	Visible light, 100 mL RhB (5 mg/L), 0.15 g sample	73% and 4 h	[121]
40 mol% $\text{CeO}_2/\text{BiVO}_4$	–	2.46	Visible light, 50 mL MB (0.02 mmol/L), 0.05 g sample	80% and 30 min	[89]
30 mol% $\text{BiVO}_4/\text{C}_3\text{N}_4$	4.52	2.45	Visible light, 50 mL RhB (0.01 mmol/L), 0.05 g sample	85% and 5 h	[97]
16.7 mol% $\text{BiVO}_4/\text{C}_3\text{N}_4$	12.99	2.25	Visible light, 100 mL MB (10 mg/L), 0.05 g sample	96% and 1 h	[98]
1 wt% GR/ BiVO_4	10	2.38	Visible light, 100 mL RhB (10 mg/L), 0.02 g sample	94% and 140 min	[122]
3 wt% GR/ BiVO_4	44.2	1.94	Visible light, 100 mL RhB (0.01 mmol/L), 0.6 mmol sample	100% and 10 min	[123]
5 wt% RGO/ BiVO_4	15.73	2.41	Visible light, 50 mL RhB (10 mg/L), 0.1 g sample	89% and 3 h	[100]
3 wt% RGO/ BiVO_4	4.84	2.32	Sunlight, 200 mL RhB (7.5 mg/L), 0.15 g sample	96.5% and 6 h	[124]
50 mol% $\text{Bi}_2\text{WO}_6/\text{BiVO}_4$	2.69	2.08	Visible light, 100 mL RhB (0.01 mmol/L), 0.1 g sample	100% and 0.5 h	[105]
3 wt% $\text{Bi}_2\text{WO}_6/\text{BiVO}_4$	–	2.50	Visible light, 50 mL phenol (10 mg/L), 0.15 g sample	81% and 6 h	[125]
2.5 wt% $\text{Cu}_2\text{O}/\text{BiVO}_4$	–	2.4	Visible light, 50 mL MB (0.02 mmol/L), 0.05 g sample	100% and 75 min	[126]
33 wt% $\text{Cu}_2\text{O}/\text{BiVO}_4$	–	2.45	Visible light, 100 mL phenol (100 mg/L), 0.2 g sample	41% and 6 h	[109]

Photocatalyst	Surface area (m ² /g)	E _g (eV)	Reaction condition	Degradation efficiency and light illumination time	References
8 wt% CuO/BiVO ₄	–	2.12	Visible light, 30 mL MO (5 mg/L), 0.03 g sample	90.4% and 3 h	[127]
1 wt% CuO/BiVO ₄	2	2.28	Visible light, 100 mL acid orange 7 (0.05 mmol/L), 0.05 g sample	95% and 3 h	[128]
Bi ₂ O ₃ /BiVO ₄ (Bi/V molar ratio = 1.1)	2.3	2.40	Sunlight, 100 mL MB (0.02 mmol/L), 0.05 g sample	100% and 40 min	[129]
Bi ₂ O ₃ /BiVO ₄	1.48	2.52	Visible light, 100 mL RhB (0.01 mmol/L), 0.1 g sample	88% and 4 h	[113]
43 mol% BiOBr/BiVO ₄	–	2.38	Visible light, 50 mL MB (10 mg/L), 0.05 g sample	97.2% and 4 h	[130]
13 mol% BiOCl/BiVO ₄	2.80	2.38	Visible light, 100 mL MO (0.0263 mmol/L), 0.1 g sample	85% and 11 h	[118]
15 mol% BiIO ₄ /BiVO ₄	–	2.40	Visible light, 50 mL RhB (0.01 mmol/L), 0.05 g sample	75% and 5 h	[131]
MoS ₂ /BiVO ₄	–	–	Visible light, 100 mL MB (40 mg/L), 0.1 g sample	195% and 2 h	[132]
80 mol% InVO ₄ /BiVO ₄	25.45	2.52	Visible light, 100 mL MB (0.02 mmol/L), 0.1 g sample	87% and 2 h	[133]
16.7 wt% Ag ₂ O/BiVO ₄	–	2.06	Visible light, 30 mL MO (5 mg/L), 0.03 g sample	91% and 160 min	[134]
22.47 wt% AgBr/BiVO ₄	–	–	Visible light, 75 mL MB (10 mg/L), 0.075 g sample	83.1% and 2.5 h	[135]
10 mol% Ag ₃ PO ₄ /BiVO ₄	–	2.46	Visible light, 100 mL MB (10 mg/L), 0.05 g sample	92% and 10 min	[136]

Table 4. Physical properties and photocatalytic activities of the BiVO₄-based heterojunction photocatalysts.

5.2. TiO₂/BiVO₄ heterojunction

As we know, TiO₂ has been widely used in environmental purification, H₂ production, photosynthesis, CO₂ reduction, etc. TiO₂ is cheap, stable, nontoxic, and environmentally friendly, and hence an ideal model for investigations of semiconductor photocatalysts [9]. However, a major drawback of TiO₂ is that only UV in the solar spectrum (about 3–5%) can be utilized to initiate the photocatalytic redox processes.

Table 4 summarizes the physical properties and photocatalytic activities of the TiO₂/BiVO₄ heterojunction samples reported in the literature. Xie et al. [88] prepared TiO₂/BiVO₄ nanocomposites with different molar ratios by impregnating BiVO₄ particles into a TiO₂ sol and after a thermal treatment at 450°C. The phenol degradation efficiency (74% after 1 h of visible-

light illumination) over the $\text{TiO}_2/\text{BiVO}_4$ nanocomposites was as 4 times as that over pure BiVO_4 . The results of the transient-state surface photovoltage responses and atmosphere-controlled steady-state surface photovoltage spectra demonstrated that the lifetime of photogenerated charge carriers over the nanosized BiVO_4 sample could be prolonged by approximately millisecond timescale after a proper molar ratio of nanocrystalline TiO_2 was coupled. The promoted charge separation was responsible for the unexpected high photocatalytic activity for phenol degradation under visible-light irradiation.

5.3. $\text{CeO}_x/\text{BiVO}_4$ heterojunction

Apart from the most commonly used TiO_2 catalyst, cubic fluorite cerium dioxide (CeO_2), a semiconductor with a bandgap energy similar to that of TiO_2 [89], shows a promising photocatalytic activity for the degradation of various organic dye pollutants [90]. CeO_2 has been used in the splitting of water for H_2 evolution and the degradation of phenol or chlorinated phenol under UV irradiation [91, 92]. However, the broad bandgap energy of CeO_2 limits its applications in visible-light illumination [92]. As we know, the heterojunction structure in composite photocatalysts can dominate photoinduced charges in the direction of transport, distance of separation, and rate of recombination, leading to the efficient separation of photogenerated charges and thus greatly improving the photocatalytic activity of the heterojunction-structured sample. If BiVO_4 is coupled with CeO_2 to form a heterojunction structure, it is possible to generate visible-light-driven catalysts that show excellent photocatalytic performance.

Wetchakun et al. [89] prepared the $\text{BiVO}_4/\text{CeO}_2$ nanocomposites by coupling a homogeneous precipitation method with a hydrothermal process. Photocatalytic activities of the as-prepared samples were examined for the degradation of MB, MO, and a mixture of MB and MO aqueous solutions under visible-light irradiation. The XRD patterns reveal that the $\text{BiVO}_4/\text{CeO}_2$ nanocomposite was composed of BiVO_4 and CeO_2 , and BiVO_4 in the composite sample was present in two crystalline phases. The sample with a $\text{BiVO}_4/\text{CeO}_2$ molar ratio of 0.6: 0.4 showed the highest photocatalytic activity (the highest MB degradation of 80% was achieved within 30 min of light irradiation). The absorption of $\text{BiVO}_4/\text{CeO}_2$ nanocomposites increased in the visible-light region (485–505 nm). Moreover, the low bandgap energy (2.46 eV) of $\text{BiVO}_4/\text{CeO}_2$ nanocomposites also influenced the dyes degradation.

The physical properties and photocatalytic activities of the $\text{CeO}_2/\text{BiVO}_4$ heterojunction samples reported in the literature are summarized in **Table 4**.

5.4. $\text{g-C}_3\text{N}_4/\text{BiVO}_4$ heterojunction

As a promising photocatalyst candidate for organic pollutant removal, graphite-like carbon nitride ($\text{g-C}_3\text{N}_4$) exhibits a relatively high photocatalytic activity under visible-light illumination due to its rapid separation of photoinduced charge carriers [93, 94]. The very negative CB (-1.13 eV) of $\text{g-C}_3\text{N}_4$ enables a strong reduction power of electrons (e^-) in the CB. Nevertheless, there are still some shortcomings (e.g., the limited visible-light absorption below 450 nm and the low surface area) for the utilization of $\text{g-C}_3\text{N}_4$ in photocatalysis [95, 96].

Recently, continuous efforts have been made to improve the photocatalytic performance of g-C₃N₄. Among these, combining g-C₃N₄ with other semiconductors to construct heterostructures can effectively promote the separation rate of photoexcited charge carriers [97]. BiVO₄ and g-C₃N₄ are selected to construct heterojunction photocatalysts according to the following considerations: (i) both BiVO₄ and g-C₃N₄ have been proved to be promising visible-light photocatalysts with desirable chemical stability and (ii) their suitable energy band alignments are beneficial for the separation of light-induced electron–hole pairs in the as-formed heterojunction photocatalysts. More importantly, the g-C₃N₄/BiVO₄ heterojunction structures can be easily modified to achieve a controllable coverage of g-C₃N₄ on BiVO₄ via a thermal annealing process, during which the g-C₃N₄ phase can be thermally etched by oxidation in air [7, 98].

Li et al. [98] prepared an efficient g-C₃N₄/BiVO₄ heterojunction photocatalyst with BiVO₄ networks decorated by discrete g-C₃N₄ nanoislands for highly efficient photocatalytic degradation of MB. There was the co-existence of BiVO₄ and g-C₃N₄ phase in the composite samples. Among these heterojunction photocatalysts, the g-C₃N₄/BiVO₄ heterojunction sample with a g-C₃N₄/BiVO₄ ratio of 15: 3 performed the best photocatalytically in the degradation of MB. In this sample, the g-C₃N₄ phase displayed a discrete nanoisland morphology (5–10 nm in diameter), which was attached tightly to the surface of BiVO₄. The as-synthesized g-C₃N₄/BiVO₄ photocatalyst showed a superior visible-light photocatalytic activity, which was about 4.5 and 6.9 times as high as that over pure BiVO₄ and g-C₃N₄, respectively. The enhanced photocatalytic activity can be ascribed to the increased charge separation efficiency, fully exposed reactive sites, and separated redox reaction sites as well as excellent visible-light response in the network composites. The physical properties and photocatalytic activities of the g-C₃N₄/BiVO₄ heterojunction samples are summarized in **Table 4**.

5.5. rGO/BiVO₄ heterojunction

Reduced graphene oxide (rGO) with excellent electrical conductivity and high carrier mobility has been proved to be an excellent media for electron transfer. The widely accepted mechanism for the enhancement in photocatalytic performance is that chemical bonding between rGO and semiconductor could accelerate the transfer of photogenerated electrons in semiconductor to rGO, thus effectively suppressing the recombination of photogenerated carriers [99]. The rGO/BiVO₄ composites have attracted much attention and significant research progress has been achieved.

Wang et al. [100] fabricated the rGO/BiVO₄ nanocomposite photocatalysts with excellent visible-light photocatalytic activities through electrostatic self-assembly via a simple surface charge modification on amorphous BiVO₄ powders with silane coupling agent. The surface areas of rGO/BiVO₄ and BiVO₄ were 23.57 and 2.62 m²/g, respectively, and their corresponding bandgap energies were 2.41 and 2.47 eV. The photocatalytic MB degradation efficiency over rGO/BiVO₄ was 94.1%, whereas that over bare BiVO₄ was just 24.1% after 30 min of visible-light irradiation. The smaller particle size with a high surface area and an increased interfacial interaction in rGO/BiVO₄ gave rise to increased photocatalytic reaction sites, extended

photoresponding range, and enhanced photogenerated charge separation and transportation efficiency.

The physical properties and photocatalytic activities of the rGO/BiVO₄ heterojunction samples reported in the literature are summarized in **Table 4**.

5.6. Bi₂WO₆/BiVO₄ heterojunction

As one of the typical Aurivillius oxides with a layered structure, Bi₂WO₆ has attracted increasing attention in many research fields due to its excellent intrinsic physicochemical properties [101], including ferroelectric piezoelectricity, pyroelectricity, catalytic activity, non-linear dielectric susceptibility, and luminescence. Besides, Bi₂WO₆ is a typical *n*-type semiconductor with a direct bandgap energy of 2.8 eV and exhibits good photocatalytic performance in the degradation of organic pollutants and the splitting of water under visible-light irradiation [102]. However, pure Bi₂WO₆ can only respond to the light with a wavelength of less than 450 nm, which accounts for a small part of solar light [103]. In addition, fast recombination of the photoinduced electron-hole pairs in Bi₂WO₆ restricts photocatalytic performance considerably [104]. Hence, to extend the range of light absorption and accelerate separation of the photogenerated charge carriers in Bi₂WO₆, a semiconductor with a low bandgap energy could be doped with Bi₂WO₆ to generate a heterojunction architecture [105]. For example, Ju et al. [105] prepared the Bi₂WO₆/BiVO₄ (C-Bi₂WO₆/BiVO₄) heterojunction photocatalyst via a hydrothermal process and after calcination at 600°C. There were co-presence of monoclinic BiVO₄ and orthorhombic Bi₂WO₆ phases, and no obvious changes in XRD peak shape and position in the calcined (C-Bi₂WO₆, C-BiVO₄, and C-Bi₂WO₆/BiVO₄) and uncalcined (Bi₂WO₆/BiVO₄) samples. The C-Bi₂WO₆/BiVO₄ sample possessed a better crystallinity than the uncalcined Bi₂WO₆/BiVO₄. The surface areas of the C-Bi₂WO₆, C-BiVO₄, Bi₂WO₆/BiVO₄, and C-Bi₂WO₆/BiVO₄ samples were 7.67, 3.62, 20.78, and 2.69 m²/g, respectively, indicating that calcination at a high temperature led to a decrease in surface area. The C-Bi₂WO₆/BiVO₄ sample exhibited a higher photocatalytic activity (RhB degradation efficiency reached 100% within 30 min of visible-light illumination) than the C-Bi₂WO₆, C-BiVO₄, or Bi₂WO₆/BiVO₄ sample. A high surface area did not give rise to a good photocatalytic activity, suggesting that there were other factors influencing the photocatalytic activity of the sample. The bandgap energies of C-Bi₂WO₆, C-BiVO₄, Bi₂WO₆/BiVO₄, and C-Bi₂WO₆/BiVO₄ were 2.69, 2.30, 2.18, and 2.08 eV, respectively. The results indicate that the C-Bi₂WO₆/BiVO₄ photocatalyst had a wider light absorption range and a more suitable bandgap energy. Based on the calculated energy bands and trapping experiment results, the authors proposed that the difference of band potentials in the two semiconductors could induce an inner electric field at the interface between Bi₂WO₆ and BiVO₄, resulting in the efficient separation of photoinduced electrons and holes on the *n-n* heterojunction and a great reduction in recombination of the photoinduced charge carriers. Therefore, the enhanced photocatalytic activity of C-Bi₂WO₆/BiVO₄ could be mainly ascribed to the effective separation of photoinduced electron-hole pairs at the heterojunction interface as well as the wider photoabsorption range and better crystallinity.

5.7. Cu₂O/BiVO₄ heterojunction

Cu₂O is a *p*-type semiconductor with a direct bandgap energy of 2.0 eV and has a noticeable light absorption capability in the visible-light region [106]. The physical properties and photocatalytic activities of the Cu₂O/BiVO₄ and CuO/BiVO₄ heterojunction samples reported in the literature are summarized in **Table 4**. For example, Yang et al. [107] reported that the Cu₂O/TiO₂ network sample showed a much higher photocatalytic activity than the pure TiO₂ sample under the irradiation of artificial solar light, and the enhanced activity of the former could be attributed to the extended absorption in the visible-light region and the effective separation of photogenerated carriers at the *p*-*n* junction interface formed between Cu₂O and TiO₂. Since the CB edge of Cu₂O is much higher than that of BiVO₄ [108], the Cu₂O/BiVO₄ composite may be an ideal system to form the *p*-*n* junction, consequently enhancing the separation of charge carriers and promoting the photocatalytic activity of BiVO₄.

Wang et al. [109] prepared the Cu₂O/BiVO₄ photocatalysts with a heterogeneous nanostructure and a *p*-*n* junction by coupling a hydrothermal process with a polyol strategy. The XRD pattern of the Cu₂O/BiVO₄ sample was quite similar to that of the pure BiVO₄ nanocrystals, and no obvious peaks due to the Cu₂O phase were detected. It can be seen from the SEM image of the Cu₂O/BiVO₄ sample that a large number of Cu₂O nanoparticles (5–20 nm in size) were assembled on the surface of the BiVO₄ nanocrystals. Under the irradiation of visible light, the photocatalytic phenol degradation efficiency (41.0%) over the Cu₂O/BiVO₄ sample was more than two times higher than that (20%) of pure BiVO₄ nanocrystals. The bandgap energies of BiVO₄ and Cu₂O/BiVO₄ were 2.48 and 2.45 eV, respectively. Therefore, the enhanced photocatalytic activity of the Cu₂O/BiVO₄ sample could be ascribed to formation of the *p*-*n* junction between *p*-type Cu₂O and *n*-type BiVO₄. The photogenerated electrons and holes were effectively separated and the recombination of electron–hole pairs was substantially suppressed. Thus, the separated electrons and holes were then free to initiate reactions with the reactants adsorbed on the photocatalyst surface, leading to an enhanced photocatalytic activity.

5.8. Bi₂O₃/BiVO₄ heterojunction

Bi₂O₃ is an active *p*-type semiconductor with an E_g of 2.7–2.8 eV [110]. **Table 4** summarizes the physical properties and photocatalytic activities of the Bi₂O₃/BiVO₄ heterojunction samples. Bessekhoud et al. [111] applied the Bi₂O₃ semiconductor to degrade orange II in water under visible-light illumination. There are few studies in the literature on the use of Bi₂O₃ as photocatalyst in the degradation of organic dyes [112]. Coupling *m*-BiVO₄ with Bi₂O₃ to form a heterojunction is an effective approach to enhance the separation of generated electron–hole pairs.

Guan et al. [113] synthesized the BiVO₄ and BiVO₄@Bi₂O₃ microspheres with a hollow olive-like morphology and a *n*-*p* core-shell structure by a sodium bis(2-ethylhexyl) sulfosuccinate (AOT)-assisted mixed solvothermal method and a NaOH etching process under hydrothermal conditions. The degradation of RhB was employed to evaluate the photocatalytic activity of the BiVO₄@Bi₂O₃ samples. The BiVO₄@Bi₂O₃ sample was composed of two phases: monoclinic scheelite BiVO₄ and cubic Bi₂O₃. Surface areas of BiVO₄ and BiVO₄@Bi₂O₃ were 1.45

and 1.48 m²/g, respectively, and their corresponding photocatalytic RhB degradation efficiencies were 42 and 88%. The results indicate that the photocatalytic activity of the sample did not depend on the surface area. The estimated bandgap energies of the BiVO₄ and BiVO₄@Bi₂O₃ were 2.43 and 2.52 eV, respectively. In order to probe the reason of enhanced photocatalytic performance, the band-edge positions of the two semiconductors were calculated. The CB-edge potential of Bi₂O₃ (0.03 eV) was more active than that of BiVO₄ (0.32 eV). Therefore, photoinduced electrons on the surface of Bi₂O₃ would easily transfer to BiVO₄ under the inducement action of the internal *p-n* electric field, leaving holes on the Bi₂O₃ VB. In such a way, the photoinduced electrons and holes could be effectively separated. Therefore, the enhanced activity of core-shell BiVO₄@Bi₂O₃ microspheres can be mostly attributed to the *p-n* heterojunction structure, thus the reducing the recombination probability of photogenerated hole–electron carriers.

5.9. BiOCl/ BiVO₄ heterojunction

In recent years, much attention has been paid on the bismuth oxyhalides (BiOX, X = Cl, Br, I) [114] and their composites in heterogeneous photocatalysis because of their characteristic hierarchical structures and unique optical properties [115]. Among them, BiOCl has drawn considerable attention as a novel photocatalyst due to their unique layered structure and high photocorrosion property [116]. However, BiOCl is similar to TiO₂, which is semiconductor with a wide bandgap E_g of 3.5 eV [117] and can only absorb UV light (less than 5% of solar energy), leading to poor photocatalytic activity under visible-light illumination.

A visible-light-active BiOCl/BiVO₄ photocatalyst with a *p-n* heterojunction structure was prepared using a hydrothermal method [118]. There were co-presence of two phases: monoclinic BiVO₄ and tetragonal BiOCl. The highest photocatalytic activity (85% MO was degraded after 11 h of visible-light irradiation) was obtained over the BiOCl/BiVO₄ heterojunction catalyst (BiOCl/BiVO₄ molar ratio = 13: 87). The surface area (2.802 m²/g) of this sample was medium in comparison with those of pure BiVO₄ (0.950 m²/g), Degussa P25 (56.000 m²/g), and other heterojunction catalysts (2.512–5.315 m²/g). The absorption edges of pure BiOCl and BiVO₄ were 360 and 520 nm, respectively. The BiOCl/BiVO₄ composites exhibited dual absorption edges at 360 and 520 nm, indicating the co-presence of BiOCl and BiVO₄. Moreover, the absorbance in the 360–520 nm range gradually decreased with increasing the BiOCl content in the BiOCl/BiVO₄ samples. Because BiOCl had negligible activity for MO degradation under visible-light irradiation, the enhanced photocatalytic activity after addition of BiOCl was due to formation of the heterojunction structure. The physical properties and photocatalytic activities of the BiOX (X = Cl, Br, I)/BiVO₄ heterojunction and other BiVO₄-based heterojunction samples are listed in **Table 4**.

6. Supported BiVO₄ photocatalyst

Due to fast recombination of photogenerated electrons and holes or lack of appropriate reaction sites, single semiconductor-based photocatalysts usually do not show high efficien-

cy in photocatalysis [9]. To improve the photocatalytic performance, it is necessary to fabricate composite photocatalysts by loading proper oxidation or reduction cocatalyst(s) on a semiconductor. In such a composite photocatalyst, the role of the cocatalyst(s) is as follows [9]: (i) providing trapping sites for the photogenerated charges and promoting the charge separation, thus enhancing the quantum efficiency; (ii) improving the photostability of the catalyst by timely consuming the photogenerated electrons and holes; and (iii) catalyzing the reactions by lowering the activation energy. Various kinds of cocatalysts have been applied to BiVO₄ to improve the photocatalytic removal of organics, including metal cocatalysts, metal oxide cocatalysts, and metal sulfide cocatalysts. As early in 2005, Kohtani et al. [137] prepared silver particles loaded on BiVO₄ by an impregnation method for the degradation of 4-*n*-alkylphenols. Since then, noble metal-loaded BiVO₄ has been widely investigated. Because the work function of a noble metal is usually larger than that of most semiconductors, electron transfer from CB of semiconductor to metal happens readily.

Chen et al. [138] prepared the Ag/BiVO₄ composites using a one-step method with ethylene glycol and water as solvent and L-lysine as surfactant. The photocatalytic performance of the composites was evaluated for the degradation of MB in an aqueous solution under visible-light irradiation. Based on the XRD and XPS results, only a small part of the Ag presented as metallic Ag (Ag⁰) dispersed on the surface of BiVO₄, whereas most of Ag was present in oxidized Ag (Ag⁺). The Ag particles with a size of about 5 nm were in close contact with BiVO₄. More than 98% of MB could be degraded over 6.5 wt% Ag/BiVO₄ within 100 min of visible-light illumination. The 6.5 wt% Ag/BiVO₄ sample had a surface area of 4.84 m²/g and a bandgap energy of 2.4 eV. The results demonstrate that a proper amount of Ag in the composite could promote the separation of photogenerated electrons and holes.

Au/BiVO₄ heterogeneous nanostructures were synthesized using a cysteine-linking strategy through the *in situ* growth of gold nanoparticles on the BiVO₄ microtubes and nanosheets [139]. Many small gold nanoparticles with an average size of 7.2 nm were dispersed on the surface of BiVO₄ microtubes or nanosheets. The bandgap energies of BiVO₄ microtubes, Au-BiVO₄ microtubes, BiVO₄ nanosheets, and Au-BiVO₄ nanosheets were 2.52, 2.51, 2.55, and 2.54 eV, respectively. The MO degradation efficiencies over the Au-BiVO₄ microtubes and nanosheets were 36 and 100% after 50 min of visible-light irradiation, respectively. However, the pure BiVO₄ microtubes and nanosheets exhibited almost no activities for MO degradation. The enhanced photocatalytic efficiency of the Au-loaded sample was attributed to two aspects: (i) the conjugated gold nanoparticles on the BiVO₄ surface might act as electron sinks to retard the recombination of the photogenerated electrons and holes in BiVO₄ so as to improve the charge separation on its surface and (ii) the surface plasmon resonance (SPR) of gold nanoparticles attached on the BiVO₄ surface can also enhance the visible-light photocatalytic efficiency.

Table 5 summarizes the physical properties and photocatalytic activities of BiVO₄-supported reduction cocatalysts reported in the literature.

Li et al. [140] prepared the CuO/BiVO₄ photocatalysts by an impregnation method. The highest MB photodegradation efficiency was obtained over the sample with a 5 atom% Cu content and after calcination at 300°C. MB could be completely degraded after 2 h of light irradiation. The

bandgap energies of pure BiVO_4 and 5 atom% CuO/BiVO_4 were 2.40 and 2.34 eV, respectively. Moreover, the surface area ($5.62 \text{ m}^2/\text{g}$) of 5 atom% CuO/BiVO_4 was higher than that ($1.89 \text{ m}^2/\text{g}$) of pure BiVO_4 . Therefore, the authors concluded that a proper Cu loading could effectively improve the photocatalytic activity.

Photocatalyst	Crystal structure	Crystallite size (nm)	Surface area (m^2/g)	E_g (eV)	Reaction condition	Degradation efficiency and light illumination time	References
6.5 wt% Ag/BiVO_4	Monoclinic	5	4.83	2.40	Visible light, 100 mL MB (0.02 mmol/L), 0.05 g sample	98% and 100 min	[138]
1.5 wt% Ag/BiVO_4	Monoclinic	10–30	–	2.10	Visible light, MB (10 mg/L), 1 g/L sample	98% and 2 h	[144]
3.5 wt% Au/BiVO_4	Monoclinic	5	–	2.54	Visible light, 10 mL MO (5 mg/L), 0.01 g sample	100% and 50 min	[139]
1 wt% Au/BiVO_4	Monoclinic	8–10	–	2.0	Visible light, 50 mL phenol (10 mg/L), 3 g/L sample	99% and 2.5 h	[145]
1 mol% CuO/BiVO_4	Monoclinic	32.7	5.62	2.34	UV light, 200 mL MB (10 mg/L), 0.2 g sample	100% and 2 h	[140]
5.0 mol% $\text{Fe}_2\text{O}_3/\text{BiVO}_4$	Monoclinic	20.38	15.27	2.38	Visible light, 50 mL MB (0.05 mmol/L), 0.05 g sample	81% and 0.5 h	[141]
0.1 wt% Pt/0.1 wt% $\text{MnO}_x/\text{BiVO}_4$	Monoclinic	–	–	–	Visible light, 100 mL MO (10 mg/L), 0.05 g sample	100% and 1.5 h	[142]
0.03 wt% Pt/0.01 wt% $\text{RuO}_2/\text{BiVO}_4$	Monoclinic	–	–	2.3	Visible light, 30 mL thiophene (600 ppm), 0.05 g sample	78% and 3 h	[143]
1 mol% $\text{Ag}_2\text{O}/\text{BiVO}_4$	Monoclinic	100	2.70	2.31	Visible light, 50 mL ibuprofen (10 mg/L), 0.04 g sample	96% and 4 h	[146]
1 wt% PdO/BiVO_4	Monoclinic	–	–	1.63	Visible light, 30 mL MO (10 mg/L), 0.2 g sample	100% and 15 h	[147]

Table 5. Physical properties and photocatalytic activities of the BiVO_4 -supported photocatalysts.

Chala et al. [141] prepared the pure BiVO_4 and Fe-loaded BiVO_4 samples by a hydrothermal method. Photocatalytic activities of the samples were examined using the degradation of MB under visible-light irradiation. The Fe/BiVO_4 sample with an optimal iron loading of 5.0 mol

% showed the best photodegradation performance (81%) within 30 min of visible-light illumination. The iron loading did not affect the crystal structure of BiVO₄, and the iron oxides (mainly Fe₂O₃) might be loaded merely on the surface of BiVO₄. The bandgap energies of BiVO₄ and 5.0 mol% Fe/BiVO₄ were 2.51 and 2.38 eV, respectively. Loading with Fe₂O₃ creates subband states in the bandgap of BiVO₄ which could then be easily excited to produce more electron-hole pairs under visible-light irradiation, hence resulting in higher photocatalytic performance. Surface areas of the pure BiVO₄ and 5.0 mol% Fe/BiVO₄ samples were 6.44 and 15.27 m²/g, respectively, indicating that loading of BiVO₄ with iron oxides led to an increase in surface area. The higher surface area could possibly provide more active sites on the catalyst surface, which gave rise to an enhancement in photocatalytic activity. The physical properties and photocatalytic activities of BiVO₄-supported oxidation cocatalysts and dual cocatalysts reported in the literature are summarized in **Table 5**.

In comparison with single cocatalyst-loaded BiVO₄ photocatalysts stated above, Li et al. [142] prepared two types of photocatalysts (*M*/MnO_{*x*}/BiVO₄ and *M*/Co₃O₄/BiVO₄, where *M* stands for noble metals) with reduction and oxidation cocatalysts by a photodeposition method for the photocatalytic degradation of MO and RhB. The photocatalytic activity of Pt/MnO_{*x*}/BiVO₄ was remarkably enhanced when Pt and MnO_{*x*} were selectively deposited on the electron-rich and hole-rich facets, which was mainly due to the synergetic effect of dual cocatalysts. Moreover, Lin et al. [143] also studied Pt-RuO₂/BiVO₄ for photocatalytic oxidation of thiophene under visible-light irradiation. The considerable enhancement in photocatalytic activity also confirmed the simultaneous presence of the reduction and oxidation cocatalysts, which was beneficial for the efficient separation and transfer of the photogenerated electrons and holes.

7. Photocatalytic degradation mechanism

7.1. Organic dyes photodegradation mechanisms

According to the literature, the main factors influencing the degradation rate of organic dyes are hydroxyl radicals ($\cdot\text{OH}$), superoxide radical ($\cdot\text{O}_2^-$), dissolved oxygen (O₂), and holes (h⁺). The mechanisms for degradation of organic dyes (such as MB, MO, and RhB) are similar. Taking an example, the photocatalytic degradation mechanism over the BiVO₄ quantum tubes-graphene composite sample for the degradation of RhB under visible-light illumination is illustrated in **Figure 11**.

It is well known that a complete photocatalytic process is generally divided into three stages: light harvesting, separation of photogenerated charges, and interfacial reactions [148]. In the photocatalytic reaction of converting dyes to CO₂ and H₂O over the BiVO₄-graphene composite material, the electrons (e⁻) are provided by photoexcitation of BiVO₄ (CB electrons). In this regard, BiVO₄ can absorb visible light to generate electron-hole pairs (reaction (1)). In fact, the photogenerated electrons instantly transfer from the CB of BiVO₄ to the carbon atoms of graphene (reaction (2)). Simultaneously, these electrons on the surface of graphene can be captured by the adsorbed O₂ molecules to produce $\cdot\text{O}_2^-$ (reaction (3)). Meanwhile, the holes on

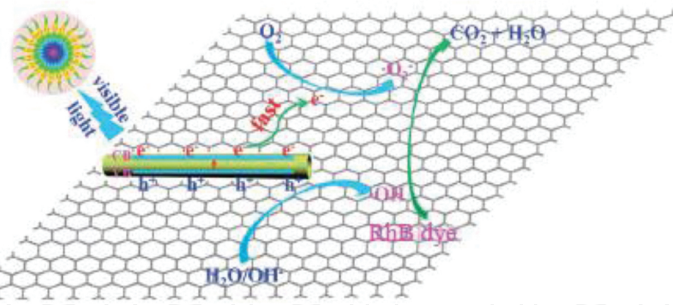
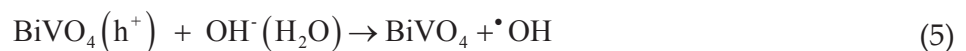
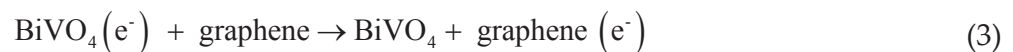
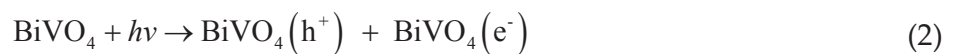


Figure 11. A schematic reaction mechanism illustrating the visible light-driven photodegradation of RhB over the *m*-BiVO₄ quantum tubes–graphene nanocomposite catalyst [123].

the surface of BiVO₄ can be scavenged by the ubiquitous H₂O molecules or OH⁻ to yield •OH radicals (reaction (4)). In this case, the RhB molecules can be subsequently destroyed into CO₂ and H₂O (reaction (5)) by the generated •O₂⁻ and •OH radicals due to their high activities [123].



It is noteworthy that holes (h⁺) can directly react with RhB molecules to generate CO₂ and H₂O (reaction (6)). Moreover, in order to improve the photocatalytic performance, H₂O₂ is often added to the dye solution as electronic sacrificial agent. It has been reported that a small amount of H₂O₂ in the initial dye solution was beneficial for trapping e⁻ to form •OH radicals (reaction (7)) and also inhibiting the recombination of e⁻/h⁺ pairs.

7.2. Phenol and its derivatives photodegradation mechanisms

The difference of degradation of phenol and its derivatives from that of degradation of organic dyes is that the intermediate products are usually generated, which are difficult to be completely degraded to CO₂ and H₂O.



There are at least 20 intermediates (see **Figure 12**) of phenol photodegradation [149], the photodegradation process of phenol is hence very complicated. Furthermore, the routes of phenol photodegradation are different under different experimental conditions. Although the active species for phenol degradation are also the $\cdot\text{OH}$, $\cdot\text{O}_2^-$, O_2 , and h^+ , phenol is difficult to be completely destroyed to CO₂ and H₂O.

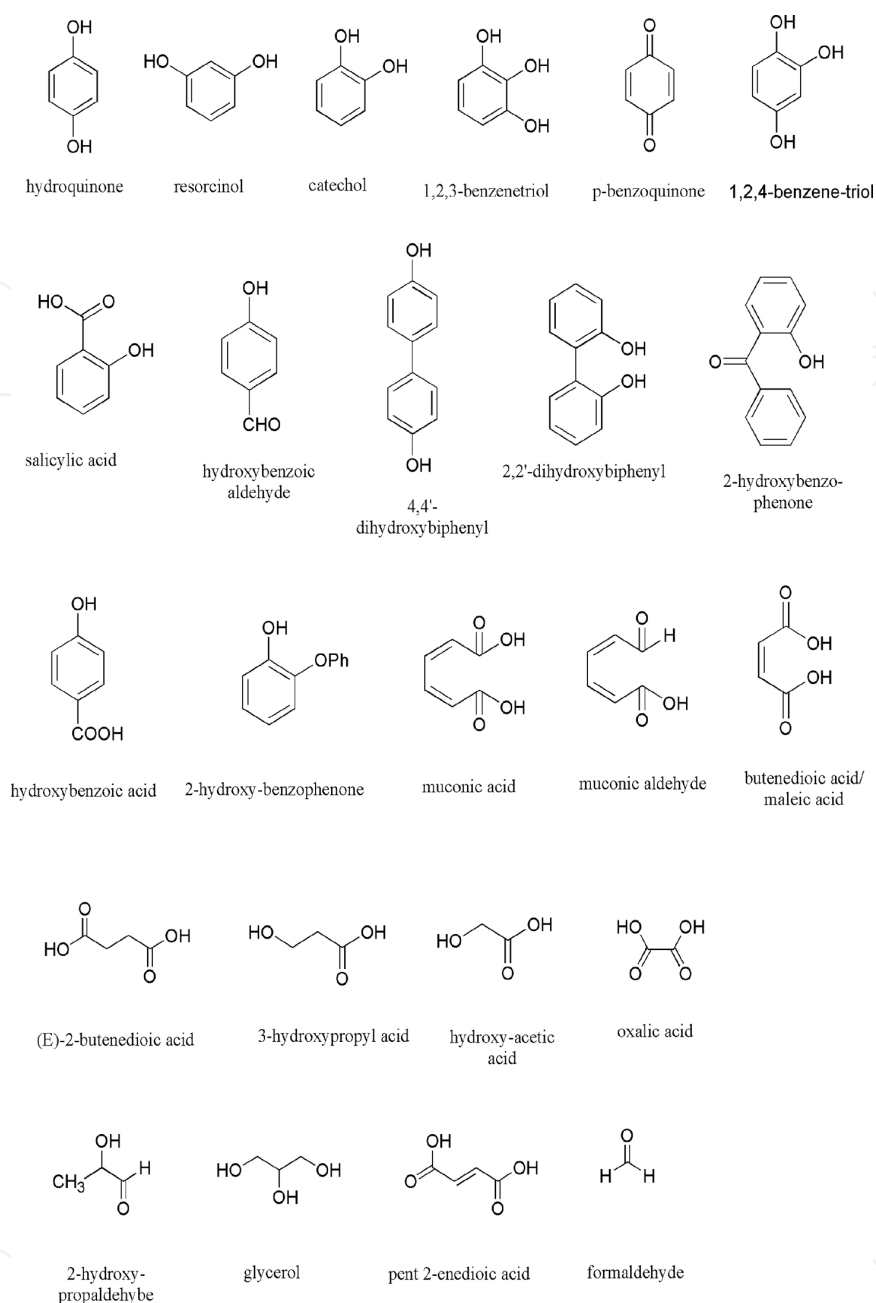


Figure 12. Chemical structures of the by-products derived from phenol photocatalytic degradation [149].

For example, Guo et al. [150] studied degradation of phenol ($C_0 = 100$ mg/L) over TiO_2 under UV light irradiation. Intermediates were analyzed with gas chromatography/mass spectrometry (GC-MS). The reaction routes were proposed, as shown in **Figure 13**. The $\cdot\text{OH}$ radicals attack the phenyl ring, yielding catechol, resorcinol, and hydroquinone, then the phenyl rings in these compounds break up to give malonic acid, the formed short-chain organic acids (such as maleic, oxalic, acetic, formic) are finally converted to CO_2 and H_2O .

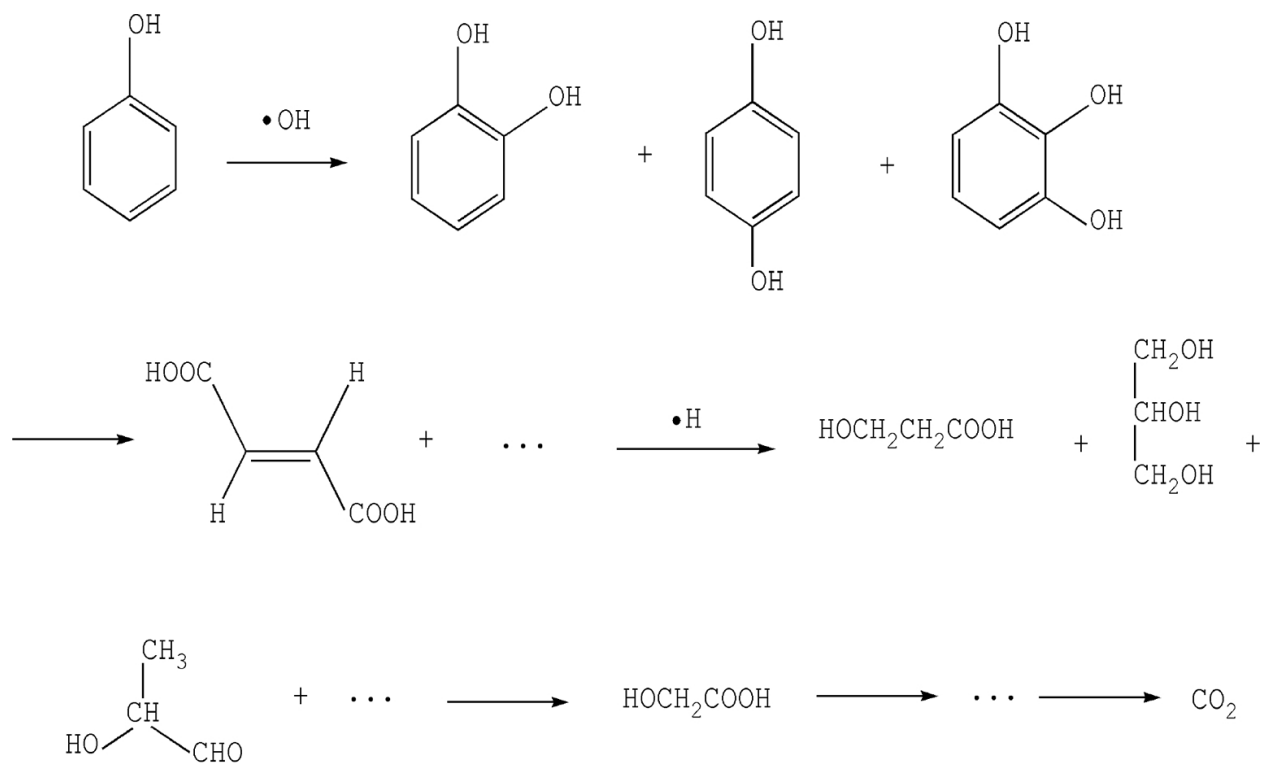


Figure 13. Phenol photodegradation route [150].

Moreover, Devi and Rajashekhar [151] also proposed a possible phenol degradation mechanism over TiO_2 under the conditions of UV light, catalyst dosage = 400 mg/L, phenol concentration = 20 mg/L, and ammonium persulfate (APS) = 100 mg/L, as shown in **Figure 14**.

Based on a plenty of literature, many possible phenol degradation mechanisms have been proposed. Unfortunately and inevitably, the by-products are always generated. It is noted that the toxicity of the by-products generated in phenol degradation processes may be stronger than phenol itself. Therefore, how to directly convert phenol into harmless products is still a big challenge.

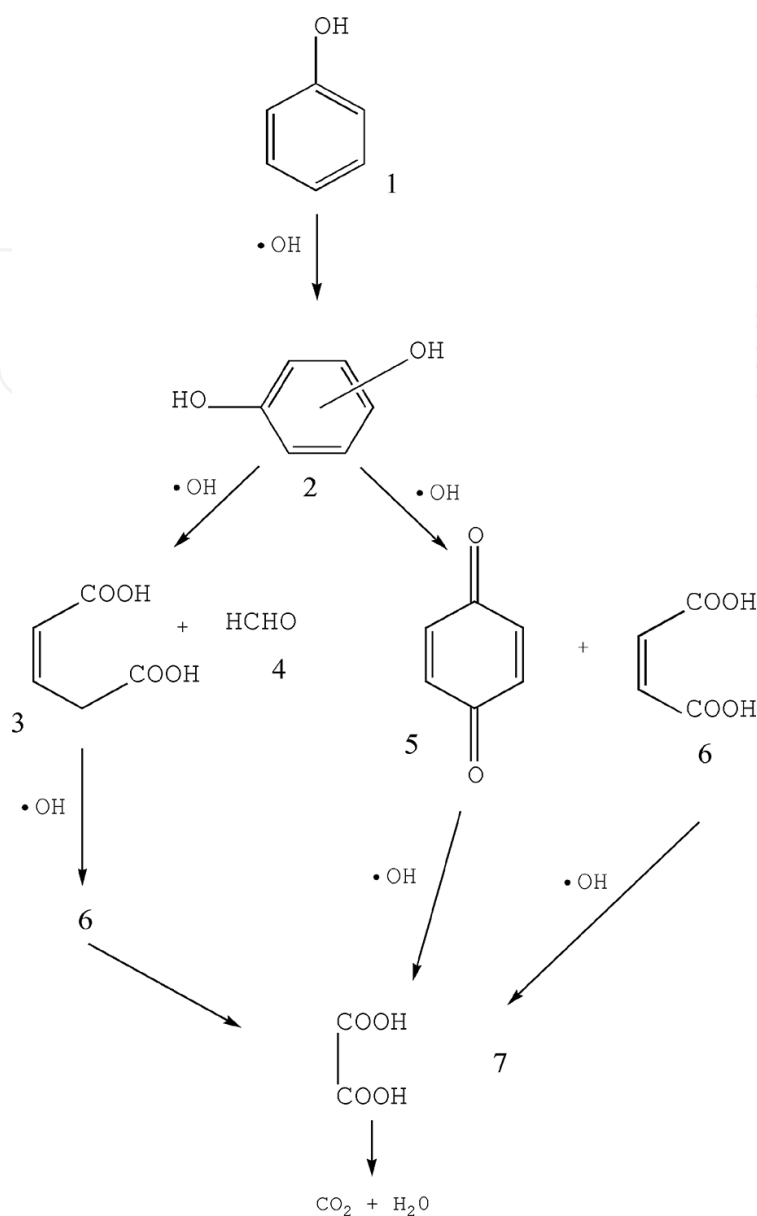


Figure 14. Phenol photodegradation mechanism [151].

8. Conclusive remarks and prospect

A large number of BiVO_4 and its related materials with different morphologies and various structures, such as well-defined morphological BiVO_4 , porous BiVO_4 , heteroatom-doped BiVO_4 , BiVO_4 -based heterojunction, and supported BiVO_4 , have been successfully synthesized in the literature. Most of them show good or even excellent photocatalytic performance for the degradation of organic dyes, phenol or its derivatives under the illumination of visible light. The structure–photocatalytic performance relationship of these materials has been established, and the involved photocatalytic degradation mechanisms have been proposed.

Due to severe situations in water contamination, researchers have devoted themselves to resolve these problems. In particular, the photocatalytic technology has attracted more and more attention because of its unique advantages. However, it has still a long way to make photocatalytic technology widely practicable. Therefore, three strategies are suggested to further improve the photocatalytic performance: (i) It is greatly desired to design and fabricate novel and highly efficient photocatalytic materials; (ii) although photocatalytic reaction mechanisms have been studied for many years, it is still difficult to identify the elementary reaction steps, therefore *in situ* characterization techniques are used to disclose the reaction mechanisms in essence; and (iii) since the photocatalytic performance can be improved significantly if light, heating, plasmon, electric or magnetic field is coupled, the synergetic effects of these energy coupling would be expected to improve the photocatalytic performance of a photocatalyst.

Author details

Kunfeng Zhang^{1,2}, Jiguang Deng^{1,2}, Yuxi Liu^{1,2}, Shaohua Xie^{1,2} and Hongxing Dai^{1,2*}

*Address all correspondence to: hxdai@bjut.edu.cn

1 Beijing Key Laboratory for Green Catalysis and Separation, Key Laboratory of Beijing on Regional Air Pollution Control, Key Laboratory of Advanced Functional Materials, Education Ministry of China, Beijing, China

2 Laboratory of Catalysis Chemistry and Nanoscience, Department of Chemistry and Chemical Engineering, College of Environmental and Energy Engineering, Beijing University of Technology, Beijing, China

References

- [1] Li HY, Sun YJ, Cai B, Gan SY, Han DX, Niu L, et al. Hierarchically Z-scheme photocatalyst of Ag@AgCl decorated on BiVO₄ (040) with enhancing photoelectrochemical and photocatalytic performance. *Applied Catalysis B: Environmental*. 2015;170–171:206–214. doi:10.1016/j.apcatb.2015.01.043
- [2] Yin WZ, Wang WZ, Zhou L, Sun SM, Zhang L. CTAB-assisted synthesis of monoclinic BiVO₄ photocatalyst and its highly efficient degradation of organic dye under visible-light irradiation. *Journal of Hazardous Materials*. 2010;173:194–199. doi:10.1016/j.jhazmat.2009.08.068
- [3] Liu YX, Dai HX, Deng JG, Zhang L, Au CT. Three-dimensional ordered macroporous bismuth vanadates: PMMA-templating fabrication and excellent visible light-driven

- photocatalytic performance for phenol degradation. *Nanoscale*. 2012;4:2317–2325. doi: 10.1039/c2nr12046a
- [4] Ni M, Leung MKH, Leung DYC, Sumathy K. A review and recent developments in photocatalytic water-splitting using TiO_2 for hydrogen production. *Renewable and Sustainable Energy Reviews*. 2007;11:401–425. doi: 10.1016/j.rser.2005.01.009
- [5] Wu Q, Han RB, Chen PF, Qi XM, Yao WF. Novel synthesis and photocatalytic performance of BiVO_4 with tunable morphologies and macroscopic structures. *Materials Science in Semiconductor Processing*. 2015;38:271–277. doi:10.1016/j.mssp.2015.04.040
- [6] Li F, Yang CY, Li QG, Cao W, Li TH. The pH-controlled morphology transition of BiVO_4 photocatalysts from microparticles to hollow microspheres. *Materials Letters*. 2015;145:52–55. doi:10.1016/j.matlet.2015.01.043
- [7] Kudo A, Omori K, Kato H. A novel aqueous process for preparation of crystal form-controlled and highly crystalline BiVO_4 powder from layered vanadates at room temperature and its photocatalytic and photophysical properties. *Journal of the American Chemical Society*. 1999;121:11459–11467. doi:10.1021/ja992541y
- [8] Nalbandian MJ, Zhang ML, Sanchez J, Choa YH, Cwiertny DM, Myung NV. Synthesis and optimization of BiVO_4 and co-catalyzed BiVO_4 nanofibers for visible light-activated photocatalytic degradation of aquatic micropollutants. *Journal of Molecular Catalysis A*. 2015;404–405:18–26. doi:10.1016/j.molcata.2015.04.003
- [9] Ma Y, Wang XL, Jia YS, Chen XB, Han HX, Li C. Titanium dioxide-based nanomaterials for photocatalytic fuel generations. *Chemical Reviews*. 2014;114:9987–10043. doi: 10.1021/cr500008u
- [10] Gao XM, Wang ZH, Fu F, Li WH. Effects of pH on the hierarchical structures and photocatalytic performance of Cu-doped BiVO_4 prepared via the hydrothermal method. *Materials Science in Semiconductor Processing*. 2015;35:197–206. doi:10.1016/j.mssp.2015.03.012
- [11] Jiang RB, Li BX, Fang CH, Wang JF. Metal/semiconductor hybrid nanostructures for plasmon-enhanced applications. *Advanced Materials*. 2014;26:5274–5309. doi:10.1002/adma.201400203
- [12] Tang JT, Song BB, Deng Q, Xin HC. Facile hydrothermal-carbonization approach to carbon-modified BiVO_4 composites with enhanced photocatalytic activity. *Materials Science in Semiconductor Processing*. 2015;35:90–95. doi: 10.1016/j.mssp.2015.01.053
- [13] Zhou B, Zhao X, Liu HJ, Qu JH, Huang CP. Synthesis of visible-light sensitive M- BiVO_4 (M = Ag, Co, and Ni) for the photocatalytic degradation of organic pollutants. *Separation and Purification Technology*. 2011;77:275–282. doi:10.1016/j.seppur.2010.12.017
- [14] Shiraishi Y, Tsukamoto D, Sugano Y, Shiro A, Ichikawa S, Tanaka S, et al. Platinum nanoparticles supported on anatase titanium dioxide as highly active catalysts for

- aerobic oxidation under visible light irradiation. *ACS Catalysis*. 2012;2:1984–1992. doi:10.1021/cs300407e
- [15] Zhang LL, Long JX, Pan WW, Zhou SY, Zhu JW, Zhao YJ, . Efficient removal of methylene blue over composite-phase BiVO₄ fabricated by hydrothermal control synthesis. *Materials Chemistry and Physics*. 2012;136:897–902. doi:10.1016/j.matchemphys.2012.08.016
- [16] Zhang X, Ai ZH, Jia FL, Zhang LZ, Fan XX, Zou ZG. Selective synthesis and visible-light photocatalytic activities of BiVO₄ with different crystalline phases. *Materials Chemistry and Physics*. 2007;103:162–167. doi:10.1016/j.matchemphys.2007.02.008
- [17] Fan HM, Jiang TF, Li HY, Wang DJ, Wang LL, Zhai JL, . Effect of BiVO₄ crystalline phases on the photoinduced carriers behavior and photocatalytic activity. *The Journal of Physical Chemistry B*. 2012;116:2425–2430. doi:10.1021/jp206798d
- [18] Walsh A, Yan Y, Huda MN, Al-Jassim MM, Wei SH. Band edge electronic structure of BiVO₄: Elucidating the role of the Bi s and V d orbitals. *Chemistry of Materials*. 2009;21:547–551. doi:10.1021/cm802894z
- [19] Park Y, McDonald KJ, Choi KS. Progress in bismuth vanadate photoanodes for use in solar water oxidation. *Chemical Society Reviews*. 2013;42:2321–2337. doi:10.1039/c2cs35260e
- [20] Ying YQ, Tao FF, Hong TJ, Wang LX. Controlled fabrication of bismuth vanadium oxide hierarchical microtubes with enhanced visible light photocatalytic activity. *Materials Science in Semiconductor Processing*. 2015;32:82–89. doi:10.1016/j.mssp.2015.01.009
- [21] Wetchakun N, Chaiwichain S, Inceesungvorn B, Pingmuang K, Phanichphant S, Minett AI, . BiVO₄/CeO₂ nanocomposites with high visible-light-induced photocatalytic activity. *ACS Applied Materials & Interfaces*. 2012;4:3718–3723. doi:10.1021/am300812n
- [22] Jiang HY, Dai HX, Meng X, Zhang L, Deng JG, Liu YX, . Hydrothermal fabrication and visible-light-driven photocatalytic properties of bismuth vanadate with multiple morphologies and/or porous structures for methyl orange degradation. *Journal of Environmental Sciences*. 2012;24:449–457. doi:10.1016/S1001-0742(11)60793-6
- [23] Thalluri SM, Hernández S, Bensaid S, Saracco G, Russo N. Green-synthesized W- and Mo-doped BiVO₄ oriented along the {040} facet with enhanced activity for the sun-driven water oxidation. *Applied Catalysis B: Environmental*. 2016;180:630–636. doi:10.1016/j.apcatb.2015.07.029
- [24] Ge L. Novel Pd/BiVO₄ composite photocatalysts for efficient degradation of methyl orange under visible light irradiation. *Materials Chemistry and Physics*. 2008;107:465–470. doi:10.1016/j.matchemphys.2007.08.016
- [25] Luo HM, Mueller AH, McCleskey TM, Burrell AK, Bauer E, Jia QX. Structural and photoelectron chemical properties of BiVO₄ thin films. *The Journal of Physical Chemistry C*. 2008;112:6099–6102. doi:10.1021/jp7113187

- [26] Wang XJ, Liu HL, Wang JR, Chang LL, Song NN, Yan ZZ, . Additive-free solvothermal preparation, characterization, and photocatalytic activity of 3D butterfly-like BiVO_4 . *Research on Chemical Intermediates*. 2015;41:2465–2477. doi:10.1007/s11164-013-1360-4
- [27] Hu LM, Dong SY, Li YK, Pi YQ, Wang JQ, Wang YK, . Controlled fabrication of monoclinic BiVO_4 rod-like structures for natural-sunlight-driven photocatalytic dye degradation. *Journal of the Taiwan Institute of Chemical Engineers*. 2014;45:2462–2468. doi:10.1016/j.jtice.2014.04.022
- [28] Xu C, Zhu GQ, Wu JL, Liang J. Template-free hydrothermal synthesis different morphologies of visible-light-driven BiVO_4 photocatalysts. *Journal of Nanoscience and Nanotechnology*. 2014;14:4475–4480. doi:10.1166/jnn.2014.8039
- [29] Kunduz S, Soylu GSP. Highly active BiVO_4 nanoparticles: The enhanced photocatalytic properties under natural sunlight for removal of phenol from wastewater. *Separation and Purification Technology*. 2015;141:221–228. doi:10.1016/j.seppur.2014.11.036
- [30] Hu Y, Li DZ, Sun FQ, Wang HB, Weng YQ, Xiong W, . One-pot template-free synthesis of heterophase BiVO_4 microspheres with enhanced photocatalytic activity. *RSC Advances*. 2015;5:54882–54889. doi:10.1039/c5ra09785a
- [31] Sun JX, Chen G, Wu JZ, Dong HJ, Xiong GH. Bismuth vanadate hollow spheres: Bubble template synthesis and enhanced photocatalytic properties for photodegradation. *Applied Catalysis B: Environmental*. 2013;132–133:304–314. doi:10.1016/j.apcatb.2012.12.002
- [32] Ma WQ, Li ZL, Liu W. Hydrothermal preparation of BiVO_4 photocatalyst with perforated hollow morphology and its performance on methylene blue degradation. *Ceramics International*. 2015;41:4340–4347. doi:10.1016/j.ceramint.2014.11.123
- [33] Castillo NC, Heel A, Graule T, Pulgarin C. Flame-assisted synthesis of nanoscale, amorphous and crystalline, spherical BiVO_4 with visible-light photocatalytic activity. *Applied Catalysis B: Environmental*. 2010;95:335–347. doi:10.1016/j.apcatb.2010.01.012
- [34] Fan HM, Wang DJ, Wang LL, Li HY, Wang P, Jiang TF, . Hydrothermal synthesis and photoelectric properties of BiVO_4 with different morphologies: an efficient visible-light photocatalyst. *Applied Surface Science*. 2011;257:7758–7762. doi:10.1016/j.apsusc.2011.04.025
- [35] Meng X, Zhang L, Dai HX, Zhao ZX, Zhang RZ, Liu YX. Surfactant-assisted hydrothermal fabrication and visible-light-driven photocatalytic degradation of methylene blue over multiple morphological BiVO_4 single-crystallites. *Materials Chemistry and Physics*. 2011;125:59–65. doi:10.1016/j.matchemphys.2010.08.071
- [36] Li HB, Liu GC, Duan XC. Monoclinic BiVO_4 with regular morphologies: Hydrothermal synthesis, characterization and photocatalytic properties. *Materials Chemistry and Physics*. 2009;115:9–13. doi:10.1016/j.matchemphys.2009.01.014

- [37] Dong SY, Feng JL, Li YK, Hu LM, Liu ML, Wang YF, . Shape-controlled synthesis of BiVO₄ hierarchical structures with unique natural-sunlight-driven photocatalytic activity. *Applied Catalysis B: Environmental*. 2014;152–153:413–424. doi:10.1016/j.apcatb.2014.01.059
- [38] Jiang HY, Dai HX, Meng X, Zhang L, Deng JG, Ji KM. Morphology-dependent photocatalytic performance of monoclinic BiVO₄ for methyl orange degradation under visible-light irradiation. *Chinese Journal of Catalysis*. 2011;32:939–949. doi:10.1016/S1872-2067(10)60215-X
- [39] Lei BX, Zeng LL, Zhang P, Sun ZF, Sun W, Zhang XX. Hydrothermal synthesis and photocatalytic properties of visible-light induced BiVO₄ with different morphologies. *Advanced Powder Technology*. 2014;25:946–951. doi:10.1016/j.appt.2014.01.014
- [40] Wang XK, Li GC, Ding J, Peng HR, Chen KZ. Facile synthesis and photocatalytic activity of monoclinic BiVO₄ micro/nanostructures with controllable morphologies. *Materials Research Bulletin*. 2012;47:3814–3818. doi:10.1016/j.materresbull.2012.04.082
- [41] Chen L, Yin SF, Huang R, Zhang Q, Luo SL, Au CT. Hollow peanut-like m-BiVO₄: facile synthesis and solar-light-induced photocatalytic property. *CrystEngComm*. 2012;14:4217–4222. doi:10.1039/c2ce06684j
- [42] Lu YJ, Shang HS, Shi FJ, Chao C, Zhang X, Zhang B. Preparation and efficient visible light-induced photocatalytic activity of m-BiVO₄ with different morphologies. *Journal of Physics and Chemistry of Solids*. 2015;85:44–50. doi:10.1016/j.jpics.2015.04.016
- [43] Obregón S, Caballero A, Colón G. Hydrothermal synthesis of BiVO₄: Structural and morphological influence on the photocatalytic activity. *Applied Catalysis B*. 2012;117–118:59–66. doi:10.1016/j.apcatb.2011.12.037
- [44] Han MD, Chen XF, Sun T, Tan O, Tse M. Synthesis of mono-dispersed m-BiVO₄ octahedral nano-crystals with enhanced visible light photocatalytic properties. *CrystEngComm*. 2011;13:6674–6679. doi:10.1039/c1ce05539a
- [45] Zhu ZF, Zhang L, Li JQ, Du J, Zhang YB, Zhou JQ. Synthesis and photocatalytic behavior of BiVO₄ with decahedral structure. *Ceramics International*. 2013;39:7461–7465. doi:10.1016/j.ceramint.2013.02.093
- [46] Chang YK, Wu YS, Lu CS, Lin PF, Wu TY. Photodegradation of alachlor using BiVO₄ photocatalyst under visible light irradiation. *Water, Air & Soil Pollution*. 2015;226:194–205. doi:10.1007/s11270-015-2452-0
- [47] Zhou L, Wang WZ, Zhang LS, Xu HL, Zhu W. Single-crystalline BiVO₄ microtubes with square cross-sections: Microstructure, growth mechanism, and photocatalytic property. *The Journal of Physical Chemistry C*. 2007;111:13659–13664. doi:10.1021/jp065155t
- [48] Ying YQ, Tao FF, Hong TJ, Wang LX. Controlled fabrication of bismuth vanadium oxide hierarchical microtubes with enhanced visible light photocatalytic activity. *Materials Science in Semiconductor Processing*. 2015;32:82–89. doi:10.1016/j.mssp.2015.01.009

- [49] Liu W, Yu YQ, Cao LX, Su G, Liu XY, Zhang L, . Synthesis of monoclinic structured BiVO₄ spindly microtubes in deep eutectic solvent and their application for dye degradation. *Journal of Hazardous Materials*. 2010;181:1102–1108. doi:10.1016/j.jhazmat.2010.05.128
- [50] Lu Y, Luo YS, Kong DZ, Zhang DY, Jia YL, Zhang XW. Large-scale controllable synthesis of dumbbell-like BiVO₄ photocatalysts with enhanced visible-light photocatalytic activity. *Journal of Solid State Chemistry*. 2012;186:255–260. doi:10.1016/j.jssc.2011.12.003
- [51] Dong L, Guo S, Zhu SY, Xu DF, Zhang LL, Huo MX, . Sunlight responsive BiVO₄ photocatalyst: Effects of pH on L-cysteine-assisted hydrothermal treatment and enhanced degradation of ofloxacin. *Catalysis Communications*. 2011;16:250–254. doi:10.1016/j.catcom.2011.05.005
- [52] Shang M, Wang WZ, Ren J, Sun SM, Zhang L. A novel BiVO₄ hierarchical nanostructure: Controllable synthesis, growth mechanism, and application in photocatalysis. *CrystEngComm*. 2010;12:1754–1758. doi:10.1039/b923115c
- [53] Ma YF, Jiang HQ, Zhang XC, Xing JB, Guan YS. Synthesis of hierarchical m-BiVO₄ particles via hydro-solvothermal method and their photocatalytic properties. *Ceramics International*. 2014;40:16485–16493. doi:10.1016/j.ceramint.2014.07.158
- [54] Obregón S, Colón G. On the different photocatalytic performance of BiVO₄ catalysts for methylene blue and rhodamine B degradation. *Journal of Molecular Catalysis A*. 2013;376:40–47. doi:10.1016/j.molcata.2013.04.012
- [55] Ke DN, Peng TY, Ma L, Cai P, Dai K. Effects of hydrothermal temperature on the microstructures of BiVO₄ and its photocatalytic O₂ evolution activity under visible light. *Inorganic Chemistry*. 2009;48:4685–4691. doi:10.1021/ic900064m
- [56] Shen Y, Huang ML, Huang Y, Lin JM, Wu JH. The synthesis of bismuth vanadate powders and their photocatalytic properties under visible light irradiation. *Journal of Alloys and Compounds*. 2010;496:287–292. doi:10.1016/j.jallcom.2010.01.144
- [57] Li GS, Zhang DQ, Yu JC. Ordered mesoporous BiVO₄ through nanocasting: A superior visible light-driven photocatalyst. *Journal of Materials Chemistry*. 2008;20:3983–3992. doi:10.1021/cm800236z
- [58] Zhou Y, Vuille K, Heel A, Probst B, Kontic R, Patzke GR. An inorganic hydrothermal route to photocatalytically active bismuth vanadate. *Applied Catalysis A*. 2010;375:140–148. doi:10.1016/j.apcata.2009.12.031
- [59] Jiang HY, Dai HX, Meng X, Ji KM, Zhang L, Deng JG. Porous olive-like BiVO₄: Alcohol-hydrothermal preparation and excellent visible-light-driven photocatalytic performance for the degradation of phenol. *Applied Catalysis B: Environmental*. 2011;105:326–334. doi:10.1016/j.apcatb.2011.04.026
- [60] Jiang HY, Meng X, Dai HX, Deng JG, Liu YX, Zhang L, . High-performance porous spherical or octapod-like single-crystalline BiVO₄ photocatalysts for the removal of

- phenol and methylene blue under visible-light illumination. *Journal of Hazardous Materials*. 2012;217–218:92–99. doi:10.1016/j.jhazmat.2012.02.073
- [61] Ge M, Liu L, Chen W, Zhou Z. Sunlight-driven degradation of rhodamine B by peanut-shaped porous BiVO₄ nanostructures in the H₂O₂-containing system. *CrystEngComm*. 2012;14:1038–1044. doi:10.1039/c1ce06264f
- [62] Wang Y, Dai HX, Deng JG, Liu YX, Zhao ZX, Li XW, . Three-dimensionally ordered macroporous InVO₄: Fabrication and excellent visible-light-driven photocatalytic performance for methylene blue degradation. *Chemical Engineering Journal*. 2013;226:87–94. doi:10.1016/j.cej.2013.04.032
- [63] Wang Y, Dai HX, Deng JG, Liu YX, Arandiyand H, Li XW. 3DOM InVO₄-supported chromia with good performance for the visible-light-driven photodegradation of rhodamine B. *Solid State Sciences*. 2013;24:62–70. doi:10.1016/j.solidstatesciences.2013.07.007
- [64] Ji KM, Deng JG, Zang HJ, Han JH, Arandiyand H, Dai HX. Fabrication and high photocatalytic performance of noble metal nanoparticles supported on 3DOM InVO₄-BiVO₄ for the visible-light-driven degradation of rhodamine B and methylene blue. *Applied Catalysis B*. 2015;165:285–295. doi:10.1016/j.apcatb.2014.10.005
- [65] Ji KM, Dai HX, Deng JG, Zang HJ, Arandiyand H, Xie SH, . 3DOM BiVO₄ supported silver bromide and noble metals: High-performance photocatalysts for the visible-light-driven degradation of 4-chlorophenol. *Applied Catalysis B: Environmental*. 2015;168–169:274–282. doi:10.1016/j.apcatb.2014.12.045
- [66] Yin C, Zhu SM, Chen ZX, Zhang W, Gu JJ, Zhang D. One step fabrication of C-doped BiVO₄ with hierarchical structures for a high-performance photocatalyst under visible light irradiation. *Journal of Materials Chemistry A*. 2013;1:8367–8378. doi:10.1039/c3ta11833a
- [67] Tan GQ, Zhang LL, Ren HJ, Huang J, Yang W, Xia A. Microwave hydrothermal synthesis of N-doped BiVO₄ nanoplates with exposed (040) facets and enhanced visible-light photocatalytic properties. *Ceramics International*. 2014;40:9541–9547. doi:10.1016/j.ceramint.2014.02.028
- [68] Li JQ, Guo ZY, Liu H, Du J, Zhu ZF. Two-step hydrothermal process for synthesis of F-doped BiVO₄ spheres with enhanced photocatalytic activity. *Journal of Alloys and Compounds*. 2013;581:40–45. doi:10.1016/j.jallcom.2013.06.141
- [69] Jiang HY, Dai HX, Deng JG, Liu YX, Zhang L, Ji KM. Porous F-doped BiVO₄: Synthesis and enhanced photocatalytic performance for the degradation of phenol under visible-light illumination. *Solid State Sciences*. 2013;17:21–27. doi:10.1016/j.solidstatesciences.2012.12.009

- [70] Guo MN, Wang Y, He QL, Wang WJ, Wang WM, Fu ZY, . Enhanced photocatalytic activity of S-doped BiVO₄ photocatalysts. *RSC Advances*. 2015;5:58633–58639. doi:10.1039/c5ra07603j
- [71] Zhao ZX, Dai HX, Deng JG, Liu YX, Au CT. Effect of sulfur doping on the photocatalytic performance of BiVO₄ under visible light illumination. *Chinese Journal of Catalysis*. 2013;34:1617–1626. doi:10.1016/S1872-2067(12)60632-9
- [72] Zhao ZX, Dai HX, Deng JG, Liu YX, Wang Y, Li XW, . Porous FeO_x/BiVO₄·S_{0.08}: Highly efficient photocatalysts for the degradation of methylene blue under visible-light illumination. *Journal of Environmental Sciences*. 2013;25:2138–2149. doi:10.1016/S1001-0742(12)60279-4
- [73] Li DZ, Wang WZ, Jiang D, Zheng YL, Li XM. Surfactant-free hydrothermal fabrication of monoclinic BiVO₄ photocatalyst with oxygen vacancies by copper doping. *RSC Advances*. 2015;5:14374–14381. doi:10.1039/C4RA14318C
- [74] Zhou B, Zhao X, Liu HJ, Qu JH, Huang CP. Visible-light sensitive cobalt-doped BiVO₄ (Co-BiVO₄) photocatalytic composites for the degradation of methylene blue dye in dilute aqueous solutions. *Applied Catalysis B: Environmental*. 2010;99:214–221. doi:10.1016/j.apcatb.2010.06.022
- [75] Obregón S, Colón G. Heterostructured Er³⁺ doped BiVO₄ with exceptional photocatalytic performance by cooperative electronic and luminescence sensitization mechanism. *Applied Catalysis B: Environmental*. 2014;158–159:242–249. doi:10.1016/j.apcatb.2014.04.029
- [76] Wang M, Che YS, Niu C, Dang MY, Dong D. Effective visible light-active boron and europium co-doped BiVO₄ synthesized by sol-gel method for photodegradation of methyl orange. *Journal of Hazardous Materials*. 2013;262:447–455. doi:10.1016/j.jhazmat.2013.08.063
- [77] Obregón S, Colón G. Excellent photocatalytic activity of Yb³⁺, Er³⁺ co-doped BiVO₄ photocatalyst. *Applied Catalysis B: Environmental*. 2014;152–153:328–334. doi:10.1016/j.apcatb.2014.01.054
- [78] Yao WF, Iwai H, Ye JH. Effects of molybdenum substitution on the photocatalytic behavior of BiVO₄. *Dalton Transactions*. 2008;11:1426–1430. doi:10.1039/b713338c
- [79] Niu ML, Zhu RS, Tian F, Song K, Cao G, Ouyang F. The effects of precursors and loading of carbon on the photocatalytic activity of C-BiVO₄ for the degradation of high concentrations of phenol under visible light irradiation. *Catalysis Today*. 2015;258:585–594. doi:10.1016/j.cattod.2015.04.005
- [80] Wang M, Zheng HY, Liu J, Dong D, Che YS, Yang CX. Enhanced visible-light-driven photocatalytic activity of B-doped BiVO₄ synthesized using a corn stem template. *Materials Science in Semiconductor Processing*. 2015;30:307–313. doi:10.1016/j.mssp.2014.09.031

- [81] Wang M, Liu Q, Che YS, Zhang LF, Zhang D. Characterization and photocatalytic properties of N-doped BiVO₄ synthesized via a sol-gel method. *Journal of Alloys and Compounds*. 2013;548:70–76. doi:10.1016/j.jallcom.2012.08.140
- [82] Chen X, Li L, Yi TT, Zhang WZ, Zhang XL, Wang LL. Microwave assisted synthesis of sheet-like Cu/BiVO₄ and its activities of various photocatalytic conditions. *Journal of Solid State Chemistry*. 2015;229:141–149. doi:10.1016/j.jssc.2015.05.026
- [83] Zhang AP, Zhang JZ. Visible-light activities of erbium doped BiVO₄ photocatalysts. *Chinese Journal of Chemical Physics*. 2010;23:73–78. doi:10.1088/1674-0068/23/01/73-78
- [84] Huang J, Tan GQ, Zhang LL, Ren HJ, Xia A, Zhao CC. Enhanced photocatalytic activity of tetragonal BiVO₄: Influenced by rare earth ion Yb³⁺. *Materials Letters*. 2014;133:20–23. doi:10.1016/j.matlet.2014.06.123
- [85] Li HY, Sun YJ, Cai B, Gan SY, Han DX, Niu L, . Hierarchically Z-scheme photocatalyst of Ag@AgCl decorated on BiVO₄ (040) with enhancing photoelectrochemical and photocatalytic performance. *Applied Catalysis B: Environmental*. 2015;170–171:206–214. doi:10.1016/j.apcatb.2015.01.043
- [86] Long M, Cai WM, Cai J, Zhou BX, Chai XY, Wu YH. Efficient photocatalytic degradation of phenol over Co₃O₄/BiVO₄ composite under visible light irradiation. *The Journal of Physical Chemistry B*. 2006;110:20211–20216. doi:10.1021/jp063441z
- [87] Yu CL, Yang K, Yu JC, Cao FF, Li X, Zhou XC. Fast fabrication of Co₃O₄ and CuO/BiVO₄ composite photocatalysts with high crystallinity and enhanced photocatalytic activity via ultrasound irradiation. *Journal of Alloys and Compounds*. 2011;509:4547–4552. doi:10.1016/j.jallcom.2011.01.100
- [88] Xie MZ, Fu XD, Jing LQ, Luan P, Feng YJ, Fu HG. Long-lived, visible-light-excited charge carriers of TiO₂/BiVO₄ nanocomposites and their unexpected photoactivity for water splitting. *Advanced Energy Materials*. 2014;4:1–6. doi:10.1002/aenm.201300995
- [89] Wetchakun N, Chaiwichain S, Inceesungvorn B, Pingmuang K, Phanichphant S, Minett AI, . BiVO₄/CeO₂ nanocomposites with high visible-light-induced photocatalytic activity. *ACS Applied Materials & Interfaces*. 2012;4:3718–3723. doi:10.1021/am300812n
- [90] Song S, Xu LJ, He ZQ, Chen JM. Mechanism of the photocatalytic degradation of C.I. reactive black 5 at pH 12.0 using SrTiO₃/CeO₂ as the catalyst. *Environmental Science & Technology*. 2007;41:5846–5853. doi: 10.1021/es070224i
- [91] Chug KH, Park DC. Water photolysis reaction on cerium oxide photocatalysts. *Catalysis Today*. 1996;30:157–162. doi:10.1016/0920-5861(96)00006-5
- [92] Valente JS, Tzompantzi F, Prince J. Highly efficient photocatalytic elimination of phenol and chlorinated phenols by CeO₂/MgAl layered double hydroxides. *Applied Catalysis B: Environmental*. 2011;102:276–285. doi:10.1016/j.apcatb.2010.12.009

- [93] Ge L, Han CC, Liu J. In situ synthesis and enhanced visible light photocatalytic activities of novel PANI-g-C₃N₄ composite photocatalysts. *Journal of Materials Chemistry*. 2012;22:11843–11850. doi:10.1039/c2jm16241e
- [94] Han CC, Ge L, Chen CF, Li YJ, Xiao XL, Zhang YN, . Novel visible light induced Co₃O₄-g-C₃N₄ heterojunction photocatalysts for efficient degradation of methyl orange. *Applied Catalysis B: Environmental*. 2014;147:546–553. doi:10.1016/j.apcatb.2013.09.038
- [95] Dong F, Wang ZY, Li YH, Ho WK, Lee SC. Immobilization of polymeric g-C₃N₄ on structured ceramic foam for efficient visible light photocatalytic air purification with real indoor illumination. *Environmental Science & Technology*. 2014;48:10345–10353. doi:10.1021/es502290f
- [96] Liu G, Niu P, Sun CH, Smith SC, Chen ZG, Lu GQ, . Unique electronic structure induced high photoreactivity of sulfur-doped graphitic C₃N₄. *Journal of the American Chemical Society*. 2010;132:11642–11648. doi:10.1021/ja103798k
- [97] Tian N, Huang HW, He Y, Guo YX, Zhang TR, Zhang YH. Mediator-free direct Z-scheme photocatalytic system: BiVO₄/g-C₃N₄ organic-inorganic hybrid photocatalyst with highly efficient visible-light induced photocatalytic activity. *Dalton Transactions*. 2015;44:4297–4307. doi:10.1039/c4dt03905j
- [98] Li CJ, Wang SP, Wang T, Wei YJ, Zhang P, Gong JL. Monoclinic porous BiVO₄ networks decorated by discrete g-C₃N₄ nano-islands with tunable coverage for highly efficient photocatalysis. *Small*. 2014;10:2783–2790. doi:10.1002/smll.201400506
- [99] Liu BQ, Liu ZF, Zhang XY, Yang LY, Zhang N, Pan GL. Polymer photovoltaic cells based on solution-processable graphene and P3HT. *Advanced Functional Materials*. 2009;19:894–904. doi:10.1002/adfm.200800954
- [100] Wang YZ, Wang W, Mao HY, Lu YH, Lu JG, Huang JY, . Electrostatic self-assembly of BiVO₄-reduced graphene oxide nanocomposites for highly efficient visible light photocatalytic activities. *ACS Applied Materials & Interfaces*. 2014;6:12698–12706. doi:10.1021/am502700p
- [101] Zhang LS, Wang HL, Chen ZG, Wong PK, Liu JS. Bi₂WO₆ micro/nano-structures: Synthesis, modifications and visible-light-driven photocatalytic applications. *Applied Catalysis B: Environmental*. 2011;106:1–13. doi:10.1016/j.apcatb.2011.05.008
- [102] Cao XF, Zhang L, Chen XT, Xue ZL. Microwave-assisted solution-phase preparation of flower-like Bi₂WO₆ and its visible-light-driven photocatalytic properties. *CrystEngComm*. 2011;13:306–311. doi:10.1039/c0ce00031k
- [103] Zhang ZJ, Wang WZ, Wang L, Sun SM. Enhancement of visible-light photocatalysis by coupling with narrow-band-gap semiconductor: A case study on Bi₂S₃/Bi₂WO₆. *ACS Applied Materials & Interfaces*. 2012;4:593–597. doi:10.1021/am2017199

- [104] Gui MS, Zhang WD, Chang YQ, Yu YX. One-step hydrothermal preparation strategy for nanostructured WO₃/Bi₂WO₆ heterojunction with high visible light photocatalytic activity. *Chemical Engineering Journal*. 2012;197:283–288. doi:10.1016/j.cej.2012.05.032
- [105] Ju P, Wang P, Li B, Fan H, Ai SY, Zhang D, . A novel calcined Bi₂WO₆/BiVO₄ heterojunction photocatalyst with highly enhanced photocatalytic activity. *Chemical Engineering Journal*. 2014;236:430–437. doi:10.1016/j.cej.2013.10.001
- [106] Fernando CAN, de Silva PHC, Wethasinha SK, Dharmadasa IM, Delsol T, Simmonds MC. Investigation of n-type Cu₂O layers prepared by a low cost chemical method for use in photovoltaic thin film solar cells. *Renewable Energy*. 2002;26:521–529. doi:10.1016/S0960-1481(01)00157-4
- [107] Yang LX, Luo SL, Li Y, Xiao Y, Kang Q, Cai QY. High efficient photocatalytic degradation of p-nitrophenol on a unique Cu₂O/TiO₂ p–n heterojunction network catalyst. *Environmental Science & Technology*. 2010;44:7641–7646. doi:10.1021/es101711k
- [108] Abdulkarem AM, Aref AA, Abdulhabeeb A, Li YF, Yu Y. Synthesis of Bi₂O₃/Cu₂O nanoflowers by hydrothermal method and its photocatalytic activity enhancement under simulated sunlight. *Journal of Alloys and Compounds*. 2013;560:132–141. doi:10.1016/j.jallcom.2013.01.134
- [109] Wang WZ, Huang XW, Wu S, Zhou YX, Wang LJ, Shi HL, . Preparation of p–n junction Cu₂O/BiVO₄ heterogeneous nanostructures with enhanced visible-light photocatalytic activity. *Applied Catalysis B: Environmental*. 2013;134–135:293–301. doi:10.1016/j.apcatb.2013.01.013
- [110] Paola AD, García-López E, Marci G, Palmisano L. A survey of photocatalytic materials for environmental remediation. *Journal of Hazardous Materials*. 2012;211–212:3–29. doi:10.1016/j.jhazmat.2011.11.050.
- [111] Bessekhoud Y, Robert D, Weber JV. Photocatalytic activity of Cu₂O/TiO₂, Bi₂O₃/TiO₂ and ZnMn₂O₄/TiO₂ heterojunctions. *Catalysis Today*. 2005;101:315–321. doi:10.1016/j.cattod.2005.03.038
- [112] Sánchez-Martínez D, Juárez-Ramírez I, Torres-Martínez LM, León-Abarte I. Photocatalytic properties of Bi₂O₃ powders obtained by an ultrasound-assisted precipitation method. *Ceramics International*. 2016;42:2013–2020. doi:10.1016/j.ceramint.2015.10.007
- [113] Guan ML, Ma DK, Hu SW, Chen YJ, Huang SM. From hollow olive-shaped BiVO₄ to n-p core-shell BiVO₄@Bi₂O₃ microspheres: Controlled synthesis and enhanced visible-light-responsive photocatalytic properties. *Inorganic Chemistry*. 2011;50:800–805. doi:10.1021/ic101961z
- [114] Wang CH, Shao CL, Liu YC, Zhang LN. Photocatalytic properties BiOCl and Bi₂O₃ nanofibers prepared by electrospinning. *Scripta Materialia*. 2008;59:332–335. doi:10.1016/j.scriptamat.2008.03.038

- [115] Zhao LJ, Zhang XC, Fan CM, Liang ZH, Han PD. First-principles study on the structural, electronic and optical properties of BiOX (X = Cl, Br, I) crystals. *Physica B*. 2012;407:3364–3370. doi:10.1016/j.physb.2012.04.039
- [116] Shenawi-Khalil S, Uvarov V, Menes E, Popov I, Sasson Y. New efficient visible light photocatalyst based on heterojunction of BiOCl–bismuth oxyhydrate. *Applied Catalysis A: General*. 2012;413–414:1–9. doi:10.1016/j.apcata.2011.10.029
- [117] Chai SY, Kim YJ, Jung MH, Chakraborty AK, Jung D, Lee WI. Heterojunctioned BiOCl/Bi₂O₃, a new visible light photocatalyst. *Journal of Catalysis*. 2009;262:144–149. doi:10.1016/j.jcat.2008.12.020
- [118] He ZQ, Shi YQ, Gao C, Wen LN, Chen JM, Song S. BiOCl/BiVO₄ p-n heterojunction with enhanced photocatalytic activity under visible-light irradiation. *The Journal of Physical Chemistry C*. 2014;118:389–398. doi:10.1021/jp409598s
- [119] Hu Y, Li DZ, Wang HB, Zeng GP, Li XH, Shao Y. Role of active oxygen species in the liquid-phase photocatalytic degradation of RhB using BiVO₄/TiO₂ heterostructure under visible light irradiation. *Journal of Molecular Catalysis A: Chemical*. 2015;408:172–178. doi:10.1016/j.molcata.2015.07.025
- [120] Zalfani M, Schueren B, Hu ZY, Rooke JC, Bourguiga R, Wu M, . Novel 3DOM BiVO₄/TiO₂ nanocomposites for highly enhanced photocatalytic activity. *Journal of Materials Chemistry A*. 2015;3:21244–21256. doi:10.1039/c5ta00783f
- [121] Xu J, Wang WZ, Wang J, Liang YJ. Controlled fabrication and enhanced photocatalytic performance of BiVO₄@CeO₂ hollow microspheres for the visible-light-driven degradation of rhodamine B. *Applied Surface Science*. 2015;349:529–537. doi:10.1016/j.apsusc.2015.04.195
- [122] Yu QQ, Tang ZR, Xu YJ. Synthesis of BiVO₄ nanosheets-graphene composites toward improved visible light photoactivity. *Journal of Energy Chemistry*. 2014;23:564–574. doi:10.1016/S2095-4956(14)60186-8
- [123] Sun YF, Qu BY, Liu Q, Gao S, Yan ZX, Yan WS, . Highly efficient visible-light-driven photocatalytic activities in synthetic ordered monoclinic BiVO₄ quantum tubes-graphene nanocomposites. *Nanoscale*. 2012;4:3761–3767. doi:10.1039/c2nr30371j
- [124] Li YK, Dong SY, Wang YF, Sun JY, Li YF, Pi YQ, . Reduced graphene oxide on a dumbbell-shaped BiVO₄ photocatalyst for an augmented natural sunlight photocatalytic activity. *Journal of Molecular Catalysis A: Chemical*. 2014;387:138–146. doi:10.1016/j.molcata.2014.02.027
- [125] Zhang XF, Gong Y, Dong XL, Zhang XX, Ma C, Shi F. Fabrication and efficient visible light-induced photocatalytic activity of Bi₂WO₆/BiVO₄ heterojunction. *Materials Chemistry and Physics*. 2012;136:472–476. doi:10.1016/j.matchemphys.2012.07.013
- [126] Yuan Q, Chen L, Xiong M, He J, Luo SL, Au CT, . Cu₂O/BiVO₄ heterostructures: synthesis and application in simultaneous photocatalytic oxidation of organic dyes and

- reduction of Cr(VI) under visible light. *Chemical Engineering Journal*. 2014;255:394–402. doi:10.1016/j.cej.2014.06.031
- [127] Li JQ, Cui MM, Guo ZY, Liu ZX, Zhu ZF. Synthesis of dumbbell-like CuO-BiVO₄ heterogeneous nanostructures with enhanced visible-light photocatalytic activity. *Materials Letters*. 2014;130:36–39. doi:10.1016/j.matlet.2014.05.084
- [128] Jang JS, Kim HG, Lee SH. Efficient photocatalytic degradation of acid orange 7 on metal oxide p–n junction composites under visible light. *Journal of Physics and Chemistry of Solids*. 2012;73:1372–1377. doi:10.1016/j.jpcs.2012.07.009
- [129] Chen L, Zhang Q, Huang R, Yin SF, Luo SL, Au CT. Porous peanut-like Bi₂O₃-BiVO₄ composites with heterojunctions: one-step synthesis and their photocatalytic properties. *Dalton Transactions*. 2012;41:9513–9518. doi:10.1039/c2dt30543g
- [130] Wu XB, Zhou HL, Gu SN, Wang FZ, Liu J, Li WJ. In situ preparation of novel heterojunction BiOBr/BiVO₄ photocatalysts with enhanced visible light photocatalytic activity. *RSC Advances*. 2015;5:92769–92777. doi:10.1039/c5ra17552f
- [131] Huang HW, Liu LY, Zhang YH, Tian N. Novel BiIO₄/BiVO₄ composite photocatalyst with highly improved visible-light-induced photocatalytic performance for rhodamine B degradation and photocurrent generation. *RSC Advances*. 2015;5:1161–1167. doi:10.1039/c4ra12916d
- [132] Li HL, Yu K, Lei X, Guo BJ, Fu H, Zhu ZQ. Hydrothermal synthesis of novel MoS₂/BiVO₄ hetero-nanoflowers with enhanced photocatalytic activity and a mechanism investigation. *The Journal of Physical Chemistry C*. 2015;119:22681–22689. doi:10.1021/acs.jpcc.5b06729
- [133] Lamdab U, Wetchakun K, Phanichphant S, Kangwansupamonkon W, Wetchakun N. Highly efficient visible light-induced photocatalytic degradation of methylene blue over InVO₄/BiVO₄ composite photocatalyst. *Journal of Materials Science*. 2015;50:5788–5798. doi:10.1007/s10853-015-9126-6
- [134] Li JQ, Cui MM, Guo ZY, Liu ZX, Zhu ZF. Preparation of p–n junction BiVO₄/Ag₂O heterogeneous nanostructures with enhanced visible-light photocatalytic activity. *Materials Letters*. 2015;151:75–78. doi:10.1016/j.matlet.2015.03.078
- [135] Song YH, Xu H, Yan J, Wang C, Cai GB, Li HM, . Preparation, characterization and photocatalytic activity of AgBr/BiVO₄ composite photocatalyst. *Journal of Nano-science and Nanotechnology*. 2014;14:6816–6823. doi:10.1166/jnn.2014.8978
- [136] Li CJ, Zhang P, Lv R, Lu JW, Wang T, Wang SP, . Selective deposition of Ag₃PO₄ on monoclinic BiVO₄ (040) for highly efficient photocatalysis. *Small*. 2013;9:3951–3956. doi:10.1002/smll.201301276
- [137] Kohtani S, Hiro J, Yamamoto N, Kudo A, Tokumura K, Nakagaki R. Adsorptive and photocatalytic properties of Ag-loaded BiVO₄ on the degradation of 4-n-alkylphenols

- under visible light irradiation. *Catalysis Communications*. 2005;6:185–189. doi:10.1016/j.catcom.2004.12.006
- [138] Chen L, Huang R, Ma YJ, Luo SL, Au CT, Yin SF. Controllable synthesis of hollow and porous Ag/BiVO₄ composites with enhanced visible-light photocatalytic performance. *RSC Advances*. 2013;3:24354–24361. doi:10.1039/c3ra43691h
- [139] Cao SW, Yin Z, Barber J, Boey FYC, Loo SCJ, Xue C. Preparation of Au-BiVO₄ heterogeneous nanostructures as highly efficient visible-light photocatalysts. *ACS Applied Materials & Interfaces*. 2012;4:418–423. doi:10.1021/am201481b
- [140] Xu H, Li HM, Wu CD, Chu JY, Yan YS, Shu HM, . Preparation, characterization and photocatalytic properties of Cu-loaded BiVO₄. *Journal of Hazardous Materials*. 2008;153:877–884. doi:10.1016/j.jhazmat.2007.09.039
- [141] Chala S, Wetchakun K, Phanichphant S, Inceesungvorn B, Wetchakun N. Enhanced visible-light-response photocatalytic degradation of methylene blue on Fe-loaded BiVO₄ photocatalyst. *Journal of Alloys and Compounds*. 2014;597:129–135. doi:10.1016/j.jallcom.2014.01.130
- [142] Li RG, Han HX, Zhang FX, Wang DE, Li C. Highly efficient photocatalysts constructed by rational assembly of dual-cocatalysts separately on different facets of BiVO₄. *Energy & Environmental Science*. 2014;7:1369–1376. doi:10.1039/c3ee43304h
- [143] Lin F, Wang DE, Jiang ZX, Ma Y, Li J, Li R, . Photocatalytic oxidation of thiophene on BiVO₄ with dual co-catalysts Pt and RuO₂ under visible light irradiation using molecular oxygen as oxidant. *Energy & Environmental Science*. 2012;5:6400–6406. doi:10.1039/c1ee02880d
- [144] Zhu GQ, Que WX. Hydrothermal synthesis and characterization of visible-light-driven dumbbell-like BiVO₄ and Ag/BiVO₄ photocatalysts. *Journal of Cluster Science*. 2013;24:531–547. doi:10.1007/s10876-012-0531-6
- [145] Long M, Jiang JJ, Li Y, Cao RQ, Zhang LY, Cai WM. Effect of gold nanoparticles on the photocatalytic and photoelectrochemical performance of Au modified BiVO₄. *Nano-Micro Letters*. 2011;3:171–177. doi:10.3786/nml.v3i3.p171-177
- [146] Bian ZY, Zhu YQ, Zhang JX, Ding AZ, Wang H. Visible-light driven degradation of ibuprofen using abundant metal-loaded BiVO₄ photocatalysts. *Chemosphere*. 2014;117:527–531. doi:10.1016/j.chemosphere.2014.09.017
- [147] Ge L. Novel Pd/BiVO₄ composite photocatalysts for efficient degradation of methyl orange under visible light irradiation. *Materials Chemistry and Physics*. 2008;107:465–470. doi:10.1016/j.matchemphys.2007.08.016
- [148] Liao GZ, Chen S, Quan X, Zhang YB, Zhao HM. Remarkable improvement of visible light photocatalysis with PANI modified core-shell mesoporous TiO₂ microspheres. *Applied Catalysis B: Environmental*. 2011;102:126–131. doi:10.1016/j.apcatb.2010.11.033

- [149] Grabowska E, Reszczyńska J, Zaleska A. Mechanism of phenol photodegradation in the presence of pure and modified-TiO₂: A review. *Water Research*. 2012;46:5453–5471. doi:10.1016/j.watres.2012.07.048
- [150] Guo ZF, Ma RX, Li GJ. Degradation of phenol by nanomaterial TiO₂ in wastewater. *Chemical Engineering Journal*. 2006;119:55–59. doi:10.1016/j.cej.2006.01.017
- [151] Devi LG, Rajashekhar KE. A kinetic model based on non-linear regression analysis is proposed for the degradation of phenol under UV/solar light using nitrogen doped TiO₂. *Journal of Molecular Catalysis A: Chemical*. 2011;334:65–76. doi:10.1016/j.molcata.2010.10.025

IntechOpen

